showed that both exogenous and endogenous AJUBA were mainly localized in the cytoplasm (Figure 4c and Supplementary Figure S3f). AJUBA transduction led to a clear increase in the YAP phosphorylation level in Y-MESO-8D cells, which was associated with an increased YAP expression level in the cytoplasm (Figure 4c). These results suggested that AJUBA suppressed YAP activity through phosphorylation and its cytoplasmic translocation in MM cells.

AJUBA inhibits cell growth of MM cell lines dependent on LATS status

To verify whether AJUBA has a growth-suppressive activity against MM cells, we carried out a cell proliferation assay. As expected, AJUBA transduction significantly inhibited cell proliferation of all three MM cell lines, NCI-H28, NCI-H290 and Y-MESO-8D, which retained both LATS1 and LATS2 expression (Figure 5a). In contrast, such significant suppression of cell proliferation was not observed in two MM cell lines, Y-MESO-14 and Y-MESO-27, which harbored *LATS2* deletion (Supplementary Figure S4a). However, there still appeared to be a difference in the proliferation curves between the latter two cell lines; AJUBA still induced a weak suppression of Y-MESO-14 cells, which retained LATS1, but not of Y-MESO-27 without LATS1 expression (Supplementary Figure S4a). The suppression levels in each MM cell line were well consistent with the YAP phosphorylation status induced by AJUBA (Figures 2a and 4a).

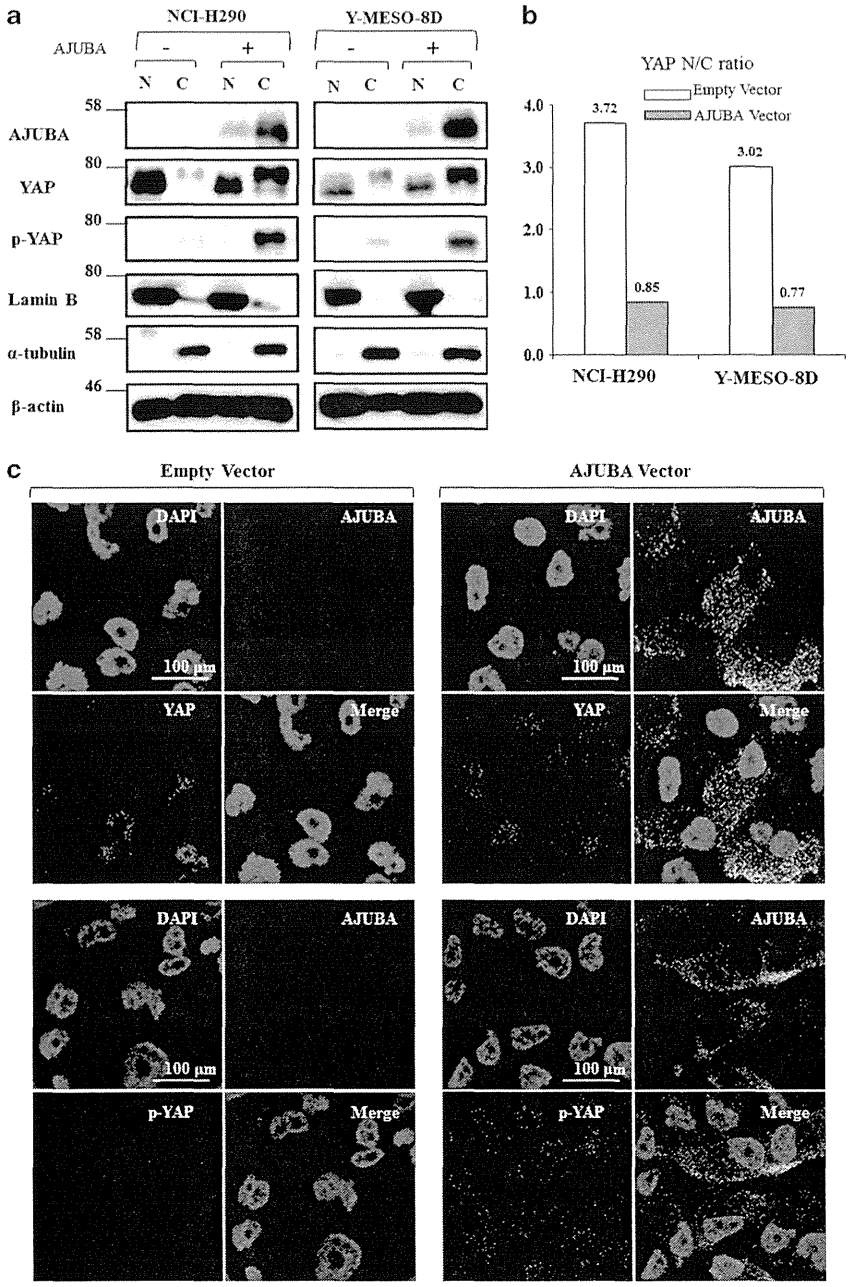

Figure 4. Subcellular localization of AJUBA and YAP. (**a**) Western blot analysis. NCI-H290 and Y-MESO-8D cells were infected with AJUBA-expressing or empty lentivirus and fractionated into nuclear and cytoplasmic fractions. AJUBA was mainly localized in the cytoplasm, and AJUBA induced a significant increase in YAP and phospho-YAP (Ser127) levels in the cytoplasm. (**b**) Nucleus/cytoplasm ratio (N/C ratio) of YAP shown in **a** is indicated with a bar graph. (**c**) Immunofluorescent microscopic analysis of Y-MESO-8D cells. Exogenous AJUBA was mainly localized in the cytoplasm of Y-MESO-8D cells infected with AJUBA-expressing lentivirus. Exogenous AJUBA induced a marked increase in total YAP and YAP phosphorylation in the cytoplasm.

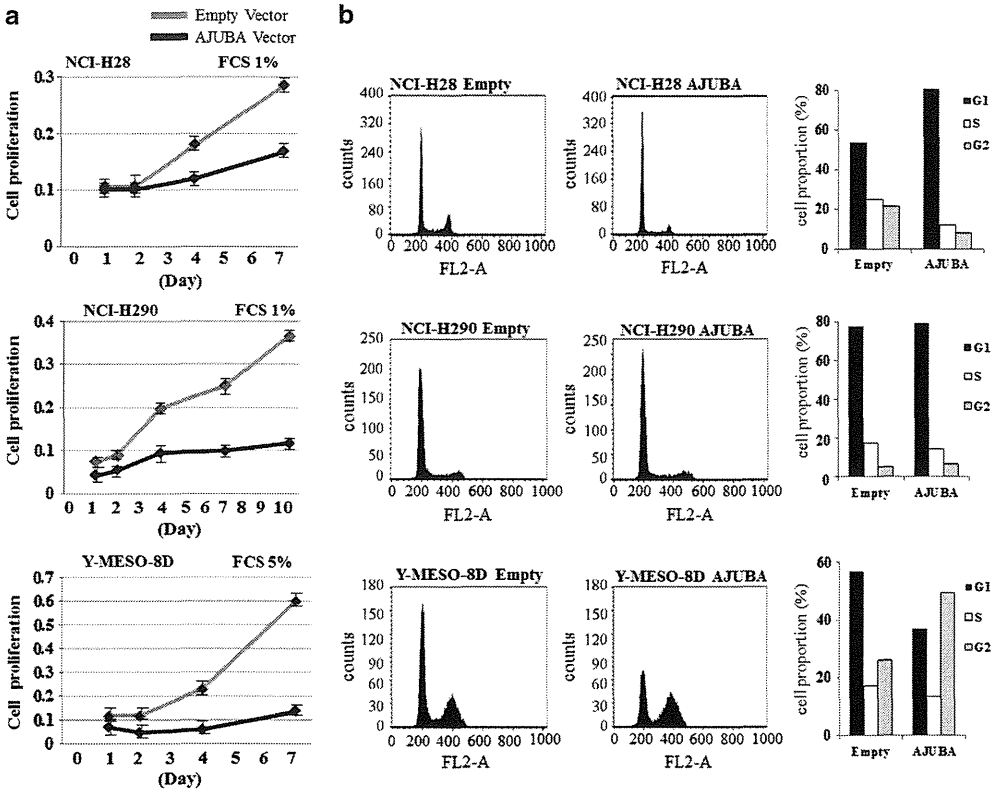

Figure 5. AJUBA inhibits cell proliferation of MM cell lines. (**a**) Cell proliferation assays. After infection with AJUBA-expressing or empty lentivirus, calorimetric assays were performed at each point. AJUBA transduction significantly inhibited the cell proliferation of NCI-H28 and NCI-H290 cells in the low-serum condition with 1% FCS and of Y-MESO-8D cells in the usual condition at 5% FCS. (**b**) Flow cytometric analyses. AJUBA transduction significantly increased cell population of G1 phase and decreased the population of S phase in NCI-H28 and NCI-H290 cells, indicating G1 arrest as an early response. Y-MESO-8D cells exhibited remarkably increased cell population of G2 phase and decreased population of S-phase, indicating G2 arrest. Average and s.d. of triplicated experiments are demonstrated in **a**.

Furthermore, we studied cell cycle profiles to elucidate the possible suppressive mechanisms of MM cell proliferation by AJUBA. Flow cytometric analyses demonstrated that the cell population of G1 phase increased, whereas that of S phase decreased, in NCI-H28 and NCI-H290 cells after infection of AJUBA-expressing lentivirus (Figure 5b). These results indicated that G1 cell cycle arrest was induced in both cell lines by exogenous AJUBA, which was consistent with the result of YAP knockdown in our previous report.[18] In contrast, Y-MESO-8D cells displayed decreased S phase and clearly increased G2 phase-cell population, suggesting that exogenous AJUBA induced G2 cell cycle arrest in this cell line. Thus, it was considered that AJUBA can induce cell cycle arrest in either G1 or G2 phase in MM cells with intact LATS1/2. Consistent with these data, LATS1 or LATS2 knockdown led to the recovery of cell proliferation in NCI-H290 cells transfected with AJUBA-expressing vector (Supplementary Figures S4c and S4d). Meanwhile, Y-MESO-14 and Y-MESO-27 cells with LATS2 deletion showed little or no change in cell populations in each cell cycle, which well accorded with marginal or no suppression of cell proliferation of these cell lines after AJUBA transduction (Supplementary Figure S4b).

We also carried out a soft agar colony formation assay. AJUBA transduction caused marked reduction in the number and size of colonies of NCI-H290 and Y-MESO-8D cells, indicating that AJUBA significantly decreased anchorage-independent growth in the presence of the LATS family (Figures 6a and b). On the other hand, similar to the results of the cell proliferation assay, AJUBA transduction induced weak or no effect on Y-MESO-14 and Y-MESO-27 cell lines, respectively.

Immunohistochemical analysis of AJUBA and YAP in primary MMs

To examine whether the frequent inactivation of AJUBA detected in MM cell lines is observed also in primary MM specimens, we carried out immunohistochemical analysis with an anti-AJUBA antibody. Among 20 cases, 5 (25%) showed negative (0) and 11 (55%) showed weak (1 +) staining of AJUBA, whereas only 4 cases showed strong (2 +) staining, indicating that AJUBA expression was frequently and consistently reduced in both MM cell lines and primary MM specimens (16 (80%); negative or weak) (Figure 7a and Supplementary Table 2). Consistent with the above results, immunohistochemical analysis also confirmed that AJUBA was mainly localized in the cytoplasm in all AJUBA-positive cases (Figure 7b).

To determine whether AJUBA downregulation is associated with YAP activation in primary MMs, we next performed immunohistochemical analysis of YAP. Among 20 cases, 13 (65%) showed that YAP was stained more strongly in the nucleus than in the cytoplasm, indicating constitutive activation of YAP (Figures 7a and b). Quite consistent with the *in vitro* results, all five cases of AJUBA-negative cases (Figure 7a and indicated in blue in Supplementary Table 2) exhibited nuclear localization of YAP, suggesting the association of AJUBA inactivation with YAP activation in primary MMs (Figures 7a and b).

DISCUSSION

In the present study, we found that AJUBA is frequently downregulated in MM cells and acts as a tumor suppressor by inducing YAP phosphorylation in a LATS family-dependent

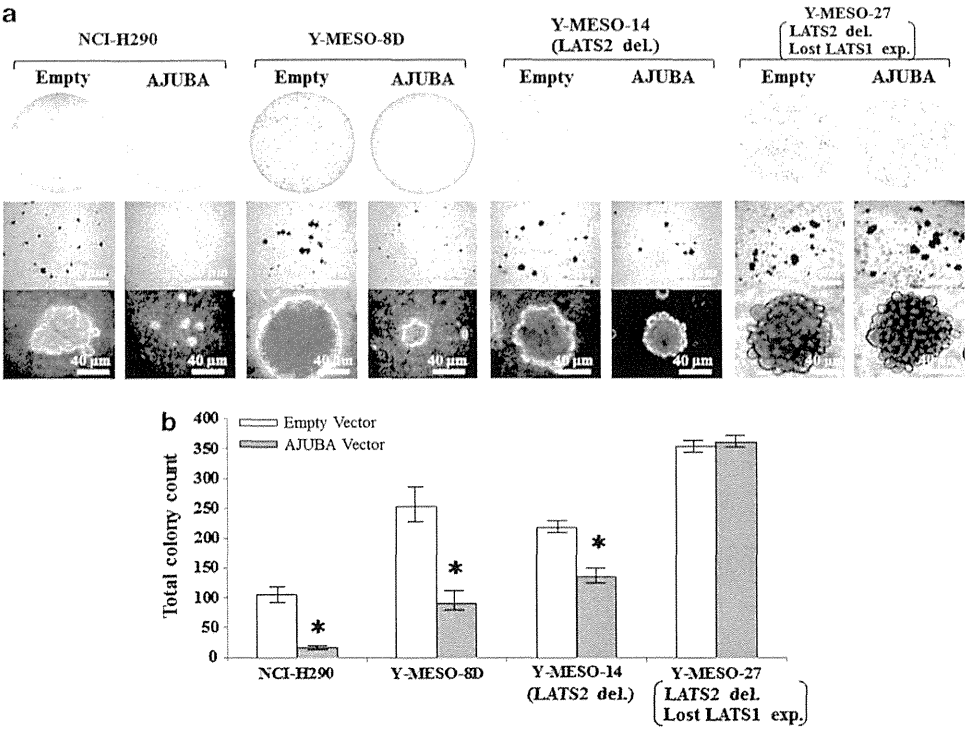

Figure 6. AJUBA suppresses anchorage-independent colony formation in MM cells. (**a**) Soft agar colony formation assays with AJUBA transduction. After 12-day incubation, colonies were stained with 0.03% crystal violet. Low (top), medium (middle) and high magnification (bottom) photos show that anchorage-independent growth was significantly suppressed in NCI-H290 and Y-MESO-8D cell lines. The size and number of colonies in the Y-MESO-14 cell line with lost LATS2 expression were moderately reduced, but not at all in the Y-MESO-27 cell line, which harbored *LATS2* deletion and low-LATS1 expression. (**b**) A graphic presentation of the soft agar colony formation assays of **a**. Average and s.d. of triplicated experiments are demonstrated in **b**. $^{*}P<0.05$ versus empty lentivirus control.

manner. Although the components of the Hippo pathway between *Drosophila* and mammals are highly conserved, our study demonstrates that AJUBA attenuates YAP activity in human MM cell lines, which contradicts its possible pro-oncogenic function in *Drosophila,* HEK293 cells and canine kidney MDCK cells.[27] In this regard, it is worth noting that RAS association domain family (RASSF) members, which are also known to be involved in the Hippo signaling pathway, regulate this pathway in opposite ways between *Drosophila* and mammals.[29,30] Furthermore, in preimplantation embryos, the Hippo signaling pathway was also shown to control cell differentiation,[31] although the Hippo pathway regulates cell proliferation by contact inhibition in cultured cells. Therefore, the tumor-suppressive function of AJUBA that we found in this study might be attributable to the evolutionary distance of gene functions and/or to the difference in cell lineage or germ layer for example, the mesothelium originates from the mesoderm.

We previously reported that the frequencies of alterations of *NF2* and *LATS2* expression in MM cell lines were about 50% and 20%, respectively.[20] However, there were several MM cell lines with YAP activation regardless of the absence of *NF2* or *LATS2* alteration. The present study revealed that all six cell lines without *NF2* or *LATS1/2* alterations showed the downregulation of AJUBA (Supplementary Table 1), suggesting that AJUBA inactivation is involved in the regulation of Hippo signaling activity. In total, 21 of 24 cell lines with YAP activation showed at least one alteration among NF2, LATS1/2 and AJUBA. Individual cell lines showed obvious single or multiple alterations of Hippo components. The difference in the target molecules also seemed to influence the levels of YAP activity. For instance, MM cells with only *NF2* inactivation showed relatively modest YAP activation (Supplementary Table 1 and Supplementary Figure S1b). This may suggest that *NF2* inactivation may not be sufficient to fully activate YAP, and thus *NF2*-defective MM cell lines frequently acquire additional alterations of other molecules such as *SAV1*, *KIBRA*, *LATS1/2* or *AJUBA* that lead to the enhancement of YAP activation (Supplementary Figures S1b and S1c). In contrast, the *LATS1/2* alteration completely disrupts the last step of the Hippo signaling cascade, resulting in significant reduction of YAP phosphorylation. Indeed, three MM cell lines with LATS1/2 inactivation but without *NF2* mutation had most activated (underphosphorylated) YAP (Supplementary Figure S1b, red columns).

Our study indicates the difference between LATS1 and LATS2 in the regulation of YAP under exogenous AJUBA transduction. Compared with three cell lines with intact LATS1/2 (Figure 2a), AJUBA transduction induced only a modest effect on YAP phosphorylation in the Y-MESO-14 cells with *LATS2* deletion and no effect in the Y-MESO-27 cells with both LATS1 and LATS2 inactivation (Figure 3a). These results were well consistent with the weaker suppression of cell proliferation and colony formation by AJUBA transduction in these cell lines (Figure 6 and Supplementary Figure S4a). Furthermore, in the MM cell lines with intact LATS1/2 that were transfected with AJUBA-expressing vector, LATS2 knockdown decreased a phosphorylated form of YAP more than did LATS1 knockdown, suggesting that LATS2 may have a more significant role. However, the effect of LATS1 knockdown could be underestimated, because silencing LATS1 resulted in increased LATS2 protein, which might enhance the difference in the effects between knockdown of LATS1 and LATS2 (Figure 3d). Thus, the possible association and stimulation mechanism between AJUBA, LATS1/2 and YAP need to be more vigorously investigated in a future study to elucidate the exact role of LATS1 on the Hippo signaling regulation. Finally, as the MM

a

AJUBA Intensity	YAP Localization		Total
	N>C	N≦C	
0	5	0	5 (25%)
1+	6	5	11 (55%)
2+	2	2	4 (20%)
Total	13 (65%)	7 (35%)	20 (100%)

b

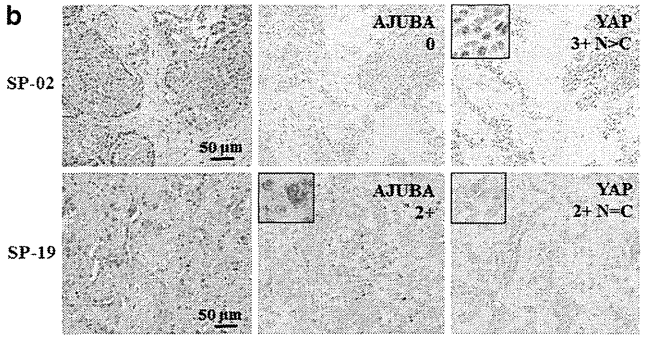

Figure 7. Immunohistochemical analyses of AJUBA and YAP in 20 primary MMs. (**a**) Twenty primary MM specimens were stained with anti-AJUBA and anti-YAP antibodies and were classified according to the YAP localization pattern (N>C or N≦C) and the staining intensity of AJUBA (negative (0), weak (1+) or strong (2+)). All 5 AJUBA-negative cases showed the nuclear localization pattern (N>C) of YAP protein. N, nucleus; C, cytoplasm. (**b**) AJUBA and YAP staining patterns of two representative cases are demonstrated. Specimen-02 showed no AJUBA expression (0) and strong nuclear staining of YAP (3+, N>C). Meanwhile, Specimen-19 had strong AJUBA expression (2+) and YAP staining in both the nucleus and the cytoplasm (2+, N=C).

cells with both LATS1 and LATS2 inactivation showed the most underphosphorylated YAP, the alteration of both LATS1 and LATS2 may be a crucial event apart from the *NF2* loss in the development of MM.

We studied the effects of AJUBA family proteins on YAP activation using the small interfering RNAs against AJUBA, LIMD1 and WTIP in the MeT-5A and Y-MESO-43 cell lines (Supplementary Figures S3a and S3b). We found that AJUBA knockdown reduced the YAP phosphorylation level, whereas LIMD1- or WTIP-knockdown led to an increase in the YAP phosphorylation level, suggesting that LIMD1 and WTIP might negatively regulate the Hippo signaling pathway, which was consistent with the previous report.[27] Moreover, in the Y-MESO-43 cell line, LIMD1- or WTIP- knockdown caused a decrease in the AJUBA expression level, by which a reduction in YAP phosphorylation levels could have been expected. However, despite the subsequent AJUBA downregulation, the YAP phosphorylation level was instead increased in this LIMD1- or WTIP-knockdown cell line. These data possibly suggest contrasting effects among AJUBA family proteins—that is, LIMD1/WTIP might counteract AJUBA and activate YAP in the MM cells. However, further studies are definitely needed to clarify the functional interactions among AJUBA family proteins on the Hippo signaling pathway in MM cells.

We found that overexpressed AJUBA induces either G1/S or G2/M arrest in MM cells. We previously reported that *FOXM1* was one of the target genes of YAP/TEAD and that YAP knockdown induces downregulation of *FOXM1*.[18] As FOXM1 is known to regulate the transcription of cell cycle-specific genes that are responsible in both G1/S and/or G2/M transition,[32–37] the cell cycle arrest induced by AJUBA might be due to FOXM1 downregulation. Interestingly, Y-MESO-8D cells predominantly presented G2 arrest induced by AJUBA. This result was consistent with a finding that the dual-luciferase reporter assay did not show a reduction of *CCND1* promoter activity in the Y-MESO-8D cell line (data not shown), suggesting that Y-MESO-8D cells have low dependency on CCND1 in G1/S progression. In addition, AJUBA has been shown to interact with multiple factors such as Aurora A, Aurora B and BUBR1.[38,39] This indicates that G2 arrest in this cell line was related to the involvement of AJUBA at the G2/M checkpoint with binding Aurora A.[38,40]

Recently, the activity of Hippo-YAP has been shown to be regulated by various factors—for example, protease-activated receptors and G-protein-coupled receptor signaling.[41,42] Mechanical signals, for example, cytoskeleton organization, cell attachment, intercellular junction and cell morphology, have also been suggested to be involved in the Hippo-YAP regulation.[43–46] In this regard, AJUBA was shown to directly interact with both α-catenin and F-actin, which were recruited at an adherent junction.[47] Thus, AJUBA might be involved in the signal transduction from mechanical signals to YAP activity, and might modulate the proliferation status of cells.

In this study, we found frequent inactivation of AJUBA in MM as well as its tumor-suppressive role that is associated with the Hippo signaling pathway. Although most MM cells show the Hippo pathway inactivation leading to constitutive activation of YAP, new treatment strategies to target this pathway may well be developed to cure patients with this highly aggressive malignancy.

MATERIALS AND METHODS

Cell lines

Eighteen Japanese MM cell lines including ACC-MESO-1, -4, Y-MESO-8D, -9, -12, -14, -22, -25, -26B, -27, -28, -29, -30, -37, -43, -45, -48 and -72 were established in our laboratory, and cells at 10–15 passages were used for each assay. Four MM cell lines including NCI-H28, NCI-H2052, NCI-H2373 and MSTO-211H, and one immortalized mesothelial cell line, MeT-5A, were purchased from the American Type Culture Collection (Rockville, MD, USA), and then used at 3–5 passages after reception. Two MM cell lines, NCI-H290 and NCI-H2452, were the kind gift of Dr Adi F Gazdar. All MM cell lines and MeT-5A were cultured in RPMI-1640 medium supplemented with 10% fetal calf serum (FCS) and 1× antibiotic–antimycotic Invitrogen (Carlsbad, CA, USA) at 37 °C in a humidified incubator with 5% CO_2.

Expression constructs and reagents

AJUBA-expressing plasmid and lentiviral vectors were constructed with pcDNA3 with Myc-tag vector (Invitrogen) or CSII-CMV-MCS-IRES2-Blasticidin vector (provided by Dr H Miyoshi, RIKEN BioResource Center). The wild-type AJUBA was amplified with cDNA synthesized from MeT-5A RNA, by reverse transcription–PCR using Pfu-Turbo DNA polymerase (Agilent Technologies, Tokyo, Japan) or PrimeSTAR Max DNA polymerase (Takara Bio, Otsu, Japan). Oligonucleotides were designed within the *AJUBA* open reading frame (*AJUBA*, 5′-ATGGAGCGGTTAGGAGAGAAAGC-3′ and 5′-TCAGATATAGTTGGCAGGGGGTTGT-3′). For luciferase reporter plasmids, *CCND1* and *CTGF* were amplified and cloned into pGL3 basic luciferase reporter vector (Promega, Madison, WI, USA) as described previously.[18,48] Rabbit anti-YAP antibody (EP1674Y) was purchased from Abcam (Tokyo, Japan). Rabbit anti-phospho-YAP (S127) antibody (#4911), anti-LATS1 antibody (#9153), anti-MST1 antibody (#3682), anti-MST2 antibody (#3952), anti-Merlin antibody (#6995), anti-AJUBA antibody (#4897) and mouse anti-CCND1 antibody (#2926) were from Cell Signaling Technology (Danvers, MA, USA). Mouse anti-AJUBA antibody (sc-374610) and anti-c-Myc antibody (sc-40), anti-α-tubulin antibody (sc-5286), goat anti-LIMD1 antibody (sc-55845) and anti-WTIP antibody (sc-24173) were from Santa Cruz (Santa Cruz, CA, USA). Mouse anti-LATS2 antibody (MAB0019) was from Abnova Corporation (Taipei, Taiwan). Rabbit anti-WWC1 (KIBRA)

antibody (HPA038016) and mouse anti-β-actin (A5441) were from Sigma (St Louis, MO, USA).

Transfection of siRNA

AJUBA, LIMD1, WTIP, LATS1, LATS2 and control small interfering RNAs (ON-TARGETplus SMARTpool siRNA reagent, Thermo Fisher Scientific, Lafayette, CO, USA) were introduced into cells by transient transfection with RNAi MAX (Invitrogen) in accordance with the manufacturer's instructions.

Cell proliferation assay

MM cells (1×10^4) were seeded on flat-bottomed 24-well plates. After 24 h, cells were transduced with lentiviral vectors, and then incubated for an additional 48 h. Cells were incubated to grow for an additional 5 days under Blasticidin (InvivoGen, San Diego, CA, USA) selection. The medium was then changed with fresh RPMI-1640 medium with 1% FCS as described previously.[19] As an exceptional case, Y-MESO-8D cells were cultured in fresh RPMI-1640 medium with 5% FCS because this cell line hardly grew in the 1% FCS medium. After an additional 24 h incubation, calorimetric assays were performed by adding 30 μl of Tetra Color One (Seikagaku, Tokyo, Japan) containing 2-(2-methoxy-4-nitrophenyl)-3-(4-nitrophenyl)-5-(2,4-disulfo
phenyl)-2H-tetrazolium, monosodium salt and 1-methoxy-5-methylphena zinium methylsulfate as electron carrier in each well and incubated at 37 °C for 1 h. Absorbance was measured at 450 nm using a multiplate reader. Cell proliferation was shown as a relative ratio to control cells.

Anchorage-independent growth in soft agar

Bottom agar was made of 1.5 ml of 0.5% agar supplemented with 10% FCS and RPMI-1640 medium, plated in 35 mm plates. Cells (3.0×10^4) were mixed with 1.0 ml of 0.35% agar supplemented with 10% FCS and RPMI-1640 medium, and then added onto the bottom agar. Cells were incubated to grow and form colonies for 12 days. Colonies were stained with 0.03% crystal violet, and the numbers of colonies were counted.

CONFLICT OF INTEREST

The authors declare no conflict of interest.

ACKNOWLEDGEMENTS

This work was supported in part by KAKENHI (24650650, 25290053), Grants-in-Aid for Third-Term Comprehensive Control Research for Cancer from the Ministry of Health, Labor and Welfare of Japan, P-DIRECT and the Takeda Science Foundation (YS). We thank Dr Adi F Gazdar for the cell lines and Mari Kizuki and Miwako Nishizawa for their excellent technical assistance. IT was supported by the Foundation for Promotion of Cancer Research.

REFERENCES

1 Pass HI, Vogelzang N, Hahn S, Carbone M. Malignant pleural mesothelioma. *Curr Probl Cancer* 2004; **28**: 93–174.
2 Yang H, Testa JR, Carbone M. Mesothelioma epidemiology, carcinogenesis, and pathogenesis. *Curr Treat Options Oncol* 2008; **9**: 147–157.
3 Delgermaa V, Takahashi K, Park EK, Le GV, Hara T, Sorahan T *et al.* Global mesothelioma deaths reported to the World Health Organization between 1994 and 2008. *Bull World Health Organ* 2011; **89**: 716–724.
4 Carbone M, Ly BH, Dodson RF, Pagano I, Morris PT, Dogan UA *et al.* Malignant mesothelioma: facts, myths, and hypotheses. *J Cell Physiol* 2012; **227**: 44–58.
5 Robinson BW, Lake RA. Advances in malignant mesothelioma. *N Engl J Med* 2005; **353**: 1591–1603.
6 Robinson BW, Musk AW, Lake RA. Malignant mesothelioma. *Lancet* 2005; **366**: 397–408.
7 Vogelzang NJ, Rusthoven JJ, Symanowski J, Denham C, Kaukel E, Ruffie P *et al.* Phase III study of pemetrexed in combination with cisplatin versus cisplatin alone in patients with malignant pleural mesothelioma. *J Clin Oncol* 2003; **21**: 2636–2644.
8 Carbone M, Kratzke RA, Testa JR. The pathogenesis of mesothelioma. *Semin Oncol* 2002; **29**: 2–17.
9 Sekido Y. Genomic abnormalities and signal transduction dysregulation in malignant mesothelioma cells. *Cancer Sci* 2010; **101**: 1–6.
10 Bianchi AB, Mitsunaga SI, Cheng JQ, Klein WM, Jhanwar SC, Seizinger B *et al.* High frequency of inactivating mutations in the neurofibromatosis type 2 gene (NF2) in primary malignant mesotheliomas. *Proc Natl Acad Sci USA* 1995; **92**: 10854–10858.
11 Sekido Y, Pass HI, Bader S, Mew DJ, Christman MF, Gazdar AF *et al.* Neurofibromatosis type 2 (NF2) gene is somatically mutated in mesothelioma but not in lung cancer. *Cancer Res* 1995; **55**: 1227–1231.
12 Dong J, Feldmann G, Huang J, Wu S, Zhang N, Comerford SA *et al.* Elucidation of a universal size-control mechanism in *Drosophila* and mammals. *Cell* 2007; **130**: 1120–1133.
13 Saucedo LJ, Edgar BA. Filling out the Hippo pathway. *Nat Rev Mol Cell Biol* 2007; **8**: 613–621.
14 Huang J, Wu S, Barrera J, Matthews K, Pan D. The Hippo signaling pathway coordinately regulates cell proliferation and apoptosis by inactivating Yorkie, the *Drosophila* Homolog of YAP. *Cell* 2005; **122**: 421–434.
15 Tapon N, Harvey KF, Bell DW, Wahrer DC, Schiripo TA, Haber D *et al.* Salvador promotes both cell cycle exit and apoptosis in *Drosophila* and is mutated in human cancer cell lines. *Cell* 2002; **110**: 467–478.
16 Badouel C, Garg A, McNeill H. Herding Hippos: regulating growth in flies and man. *Curr Opin Cell Biol* 2009; **21**: 837–843.
17 Zhao B, Ye X, Yu J, Li L, Li W, Li S *et al.* TEAD mediates YAP-dependent gene induction and growth control. *Genes Dev* 2008; **22**: 1962–1971.
18 Mizuno T, Murakami H, Fujii M, Ishiguro F, Tanaka I, Kondo Y *et al.* YAP induces malignant mesothelioma cell proliferation by upregulating transcription of cell cycle-promoting genes. *Oncogene* 2012; **31**: 5117–5122.
19 Yokoyama T, Osada H, Murakami H, Tatematsu Y, Taniguchi T, Kondo Y *et al.* YAP1 is involved in mesothelioma development and negatively regulated by Merlin through phosphorylation. *Carcinogenesis* 2008; **29**: 2139–2146.
20 Murakami H, Mizuno T, Taniguchi T, Fujii M, Ishiguro F, Fukui T *et al.* LATS2 is a tumor suppressor gene of malignant mesothelioma. *Cancer Res* 2011; **71**: 873–883.
21 Feng Y, Longmore GD. The LIM protein Ajuba influences interleukin-1-induced NF-kappaB activation by affecting the assembly and activity of the protein kinase Czeta/p62/TRAF6 signaling complex. *Mol Cell Biol* 2005; **25**: 4010–4022.
22 Locasale JW, Shaw AS, Chakraborty AK. Scaffold proteins confer diverse regulatory properties to protein kinase cascades. *Proc Natl Acad Sci USA* 2007; **104**: 13307–13312.
23 Shaw AS, Filbert EL. Scaffold proteins and immune-cell signalling. *Nat Rev Immunol* 2009; **9**: 47–56.
24 Levchenko A, Bruck J, Sternberg PW. Scaffold proteins may biphasically affect the levels of mitogen-activated protein kinase signaling and reduce its threshold properties. *Proc Natl Acad Sci USA* 2000; **97**: 5818–5823.
25 Burack WR, Shaw AS. Signal transduction: hanging on a scaffold. *Curr Opin Cell Biol* 2000; **12**: 211–216.
26 Abe Y, Ohsugi M, Haraguchi K, Fujimoto J, Yamamoto T. LATS2-Ajuba complex regulates gamma-tubulin recruitment to centrosomes and spindle organization during mitosis. *FEBS Lett* 2006; **580**: 782–788.
27 Das Thakur M, Feng Y, Jagannathan R, Seppa MJ, Skeath JB, Longmore GD *et al.* Ajuba LIM proteins are negative regulators of the Hippo signaling pathway. *Curr Biol* 2010; **20**: 657–662.
28 Zhao B, Wei X, Li W, Udan RS, Yang Q, Kim J *et al.* Inactivation of YAP oncoprotein by the Hippo pathway is involved in cell contact inhibition and tissue growth control. *Genes Dev* 2007; **21**: 2747–2761.
29 Oh HJ, Lee KK, Song SJ, Jin MS, Song MS, Lee JH *et al.* Role of the tumor suppressor RASSF1A in Mst1-mediated apoptosis. *Cancer Res* 2006; **66**: 2562–2569.
30 Polesello C, Huelsmann S, Brown NH, Tapon N. The *Drosophila* RASSF homolog antagonizes the hippo pathway. *Curr Biol* 2006; **16**: 2459–2465.
31 Sasaki H. Mechanisms of trophectoderm fate specification in preimplantation mouse development. *Dev Growth Differ* 2010; **52**: 263–273.
32 Alvarez-Fernandez M, Halim VA, Krenning L, Aprelia M, Mohammed S, Heck AJ *et al.* Recovery from a DNA-damage-induced G2 arrest requires Cdk-dependent activation of FoxM1. *EMBO Rep* 2010; **11**: 452–458.
33 Laoukili J, Stahl M, Medema RH. FoxM1: at the crossroads of ageing and cancer. *Biochim Biophys Acta* 2007; **1775**: 92–102.
34 Wang IC, Chen YJ, Hughes D, Petrovic V, Major ML, Park HJ *et al.* Forkhead box M1 regulates the transcriptional network of genes essential for mitotic progression and genes encoding the SCF (Skp2-Cks1) ubiquitin ligase. *Mol Cell Biol* 2005; **25**: 10875–10894.
35 Fu Z, Malureanu L, Huang J, Wang W, Li H, van Deursen JM *et al.* Plk1-dependent phosphorylation of FoxM1 regulates a transcriptional programme required for mitotic progression. *Nat Cell Biol* 2008; **10**: 1076–1082.

36 Wang IC, Chen YJ, Hughes DE, Ackerson T, Major ML, Kalinichenko VV *et al.* FoxM1 regulates transcription of JNK1 to promote the G1/S transition and tumor cell invasiveness. *J Biol Chem* 2008; **283**: 20770–20778.
37 Wang Z, Banerjee S, Kong D, Li Y, Sarkar FH. Down-regulation of Forkhead Box M1 transcription factor leads to the inhibition of invasion and angiogenesis of pancreatic cancer cells. *Cancer Res* 2007; **67**: 8293–8300.
38 Hirota T, Kunitoku N, Sasayama T, Marumoto T, Zhang D, Nitta M *et al.* Aurora-A and an interacting activator, the LIM protein Ajuba, are required for mitotic commitment in human cells. *Cell* 2003; **114**: 585–598.
39 Ferrand A, Chevrier V, Chauvin JP, Birnbaum D. Ajuba: a new microtubule-associated protein that interacts with BUBR1 and Aurora B at kinetochores in metaphase. *Biol Cell* 2009; **101**: 221–235.
40 Benzinger A, Muster N, Koch HB, Yates 3rd JR, Hermeking H. Targeted proteomic analysis of 14-3-3 sigma, a p53 effector commonly silenced in cancer. *Mol Cell Proteomics* 2005; **4**: 785–795.
41 Mo JS, Yu FX, Gong R, Brown JH, Guan KL. Regulation of the Hippo-YAP pathway by protease-activated receptors (PARs). *Genes Dev* 2012; **26**: 2138–2143.
42 Yu FX, Zhao B, Panupinthu N, Jewell JL, Lian I, Wang LH *et al.* Regulation of the Hippo-YAP pathway by G-protein-coupled receptor signaling. *Cell* 2012; **150**: 780–791.
43 Zhao B, Li L, Wang L, Wang CY, Yu J, Guan KL *et al.* Cell detachment activates the Hippo pathway via cytoskeleton reorganization to induce anoikis. *Genes Dev* 2012; **26**: 54–68.
44 Boggiano JC, Fehon RG. Growth control by committee: intercellular junctions, cell polarity, and the cytoskeleton regulate Hippo signaling. *Dev Cell* 2012; **22**: 695–702.
45 Wada K, Itoga K, Okano T, Yonemura S, Sasaki H. Hippo pathway regulation by cell morphology and stress fibers. *Development* 2011; **138**: 3907–3914.
46 Sansores-Garcia L, Bossuyt W, Wada K, Yonemura S, Tao C, Sasaki H *et al.* Modulating F-actin organization induces organ growth by affecting the Hippo pathway. *EMBO J* 2011; **30**: 2325–2335.
47 Marie H, Pratt SJ, Betson M, Epple H, Kittler JT, Meek L *et al.* The LIM protein Ajuba is recruited to cadherin-dependent cell junctions through an association with alpha-catenin. *J Biol Chem* 2003; **278**: 1220–1228.
48 Fujii M, Toyoda T, Nakanishi H, Yatabe Y, Sato A, Matsudaira Y *et al.* TGF-beta synergizes with defects in the Hippo pathway to stimulate human malignant mesothelioma growth. *J Exp Med* 2012; **209**: 479–494.

Supplementary Information accompanies this paper on the Oncogene website (http://www.nature.com/onc)

Carcinogenesis vol.35 no.1 pp.164–172, 2014
doi:10.1093/carcin/bgt267
Advance Access publication July 19, 2013

Cancer-promoting role of adipocytes in asbestos-induced mesothelial carcinogenesis through dysregulated adipocytokine production

Shan Hwu Chew[1], Yasumasa Okazaki[1], Hirotaka Nagai[1,2], Nobuaki Misawa[1], Shinya Akatsuka[1], Kyoko Yamashita[1], Li Jiang[1], Yoriko Yamashita[1], Michio Noguchi[3], Kiminori Hosoda[3,4], Yoshitaka Sekido[5], Takashi Takahashi[6] and Shinya Toyokuni[1,*]

[1]Department of Pathology and Biological Responses, Nagoya University Graduate School of Medicine, Nagoya 466-8550, Japan, [2]Department of Pathology and Biology of Diseases, [3]Department of Endocrinology and Metabolism and [4]Faculty of Human Health Science, Kyoto University Graduate School of Medicine, Kyoto 606-8315, Japan, [5]Division of Molecular Oncology, Aichi Cancer Center Research Institute, Nagoya 464-8681, Japan and [6]Department of Molecular Carcinogenesis, Nagoya University Graduate School of Medicine, Nagoya 466-8550, Japan

*To whom correspondence should be addressed. Tel: +81 52 744 2086; Fax: +81 52 744 2091;
Email: toyokuni@med.nagoya-u.ac.jp

Like many other human cancers, the development of malignant mesothelioma is closely associated with a chronic inflammatory condition. Both macrophages and mesothelial cells play crucial roles in the inflammatory response caused by asbestos exposure. Here, we show that adipocytes can also contribute to asbestos-induced inflammation through dysregulated adipocytokine production. 3T3-L1 preadipocytes were differentiated into mature adipocytes prior to use. These cells took up asbestos fibers (chrysotile, crocidolite and amosite) but were more resistant to asbestos-induced injury than macrophages and mesothelial cells. Expression microarray analysis followed by reverse transcription–PCR revealed that adipocytes respond directly to asbestos exposure with an increased production of proinflammatory adipocytokines [e.g. monocyte chemoattractant protein-1 (MCP-1)], whereas the production of anti-inflammatory adipocytokines (e.g. adiponectin) is suppressed. This was confirmed in epididymal fat pad of mice after intraperitoneal injection of asbestos fibers. Such dysregulated adipocytokine production favors the establishment of a proinflammatory environment. Furthermore, MCP-1 marginally promoted the growth of MeT-5A mesothelial cells and significantly enhanced the wound healing of Y-MESO-8A and Y-MESO-8D human mesothelioma cells. Our results suggest that increased levels of adipocytokines, such as MCP-1, can potentially contribute to the promotion of mesothelial carcinogenesis through the enhanced recruitment of inflammatory cells as well as a direct growth and migration stimulatory effect on mesothelial and mesothelioma cells. Taken together, our findings support a potential cancer-promoting role of adipocytes in asbestos-induced mesothelial carcinogenesis.

Introduction

Malignant mesothelioma, which arises from the mesothelial cells lining the pleural, peritoneal and pericardial cavity, is closely associated with exposure to asbestos fibers. The first convincing evidence of an etiologic relationship between asbestos fibers and malignant mesothelioma emerged in 1960 (1). Since then, there has been considerable interest in unraveling the mechanisms underlying asbestos-induced mesothelial carcinogenesis. Macrophages were the first to receive great attention, as asbestos exposure is often associated with a chronic granulomatous inflammatory response. Several groups reported the activation of macrophages by asbestos fibers, and they showed that asbestos fibers were able to induce macrophages to release a multitude of factors, such as lysosomal enzymes, cytokines, plasminogen activators and reactive oxygen species (2–4), which collectively contribute to chronic inflammation. Subsequent studies revealed a direct interaction between asbestos fibers and mesothelial cells, and asbestos fibers were shown to be able to activate certain signaling cascades within mesothelial cells. This activation might be critical for mesothelial transformation (5–8). In addition, mesothelial cells themselves also play a role in the inflammatory response. Mesothelial cells are particularly sensitive to the cytotoxic effect of asbestos fibers. Yang *et al.* (9) termed the process of asbestos-induced mesothelial cell death as 'programmed necrosis', and they reported that during this process, there was an extensive release of high-mobility group box 1 into the extracellular space, which then initiated a chronic inflammatory response by inducing the macrophages to release tumor necrosis factor-α. Together, this evidence strongly supports the vital role of chronic inflammation in asbestos carcinogenicity.

To establish an animal model of mesothelioma, asbestos fibers are usually injected into the pleural or peritoneal cavity (10–12). According to some previous reports, the peritoneal cavity appeared to be more sensitive to the effect of asbestos fibers compared with the pleural cavity, i.e. malignant mesothelioma developed more frequently and rapidly in the peritoneal cavity following asbestos injection (13,14). We speculated that this finding might be related to the abundance of adipose tissue in the peritoneal cavity. A substantial body of recent evidence has revealed the role of adipose tissue in inflammation, particularly in obesity-related inflammation (15–17). This inflammatory response in the adipose tissue of obese individuals is linked to the development of type 2 diabetes mellitus.

Adipose tissue is now recognized as an endocrine organ that is capable of secreting a wide variety of biologically active peptides collectively known as adipocytokines [e.g. monocyte chemoattractant protein-1 (MCP-1), interleukin-6 (IL-6), leptin, adiponectin, plasminogen activator inhibitor-1 (PAI-1), resistin and visfatin]. Evidence from numerous epidemiologic studies has revealed an increased risk of cancer development in obese individuals, further supporting a cancer-promoting role of adipose tissue (18–21). Obesity has been defined as a low-grade chronic inflammatory condition. Many groups have reported that the dysregulated endocrine function of adipose tissue underlies this obesity-related inflammation (22–25). Dysregulation of adipose tissue generally results in the enhanced production of proinflammatory adipocytokines and suppression of anti-inflammatory adipocytokines.

Some previous studies have demonstrated the ability of adipocytes to perform phagocytosis in a macrophage-like manner (26,27). A direct interaction between asbestos fibers and adipocytes involving fiber internalization is thus very likely to take place. We hypothesized that this interaction can trigger off an inflammatory response in adipocytes which occurs through dysregulation of adipocytokine production, as in obesity. Due to the close anatomic proximity between adipocytes and mesothelial cells, altered levels of adipocytokines can potentially affect mesothelial cells in a paracrine manner. We performed this study to evaluate the potential involvement of adipose tissue as a cancer promoter in asbestos-induced carcinogenesis through its ability to aggravate the inflammatory response.

Abbreviations: Ccl, chemokine C-C motif ligand; FBS, fetal bovine serum; IL-6, interleukin-6; MCP-1, monocyte chemoattractant protein-1; mRNA, messenger RNA; MTT, thiazolyl blue tetrazolium bromide; NT-tngl, tangled carbon nanotubes; PAI-1, plasminogen activator inhibitor-1; Prl2c5, prolactin family 2, subfamily c, member 5; RT–PCR, reverse transcription–PCR.

Materials and methods

Materials

Three types of Union for International Cancer Control asbestos fibers (chrysotile A, crocidolite and amosite) were suspended in physiological saline. Tangled carbon nanotubes (NT-tngl, diameter = 15 nm; VGCF-X, Showa Denko, Tokyo, Japan) were suspended in physiological saline containing 0.5% bovine serum albumin. The 3T3-L1 preadipocyte cell line was a kind gift from Dr M.N. and Prof. K.H. (Kyoto University, Kyoto, Japan). MeT-5A and RAW264.7 cell lines were obtained from American Type Culture Collection (Manassas, VA). Y-MESO-8A and Y-MESO-8D cell lines were kindly provided by Prof. Y.S. (Aichi Cancer Centre Research Institute, Nagoya, Japan). These two human mesothelioma cell lines were established from the same Japanese patient with biphasic-like characteristics of malignant pleural mesothelioma and they showed epithelial and sarcomatous phenotypes, respectively, in cell culture (28). Recombinant human MCP-1 was purchased from PeproTech (Rocky Hill, NJ). Thiazolyl blue tetrazolium bromide (MTT) was purchased from Sigma (St Louis, MO). Dimethyl sulfoxide was purchased from Wako (Osaka, Japan).

Cell culture

3T3-L1 preadipocytes were maintained in Dulbecco's modified Eagle's medium supplemented with 10% calf serum and antibiotics. The differentiation of these preadipocytes into mature adipocytes was induced with Dulbecco's modified Eagle's medium supplemented with 10% fetal bovine serum (FBS), 0.5 mM 3-isobutyl-1-methyl-xanthine, 0.25 μM dexamethasone and 1 μg/ml insulin. Mature adipocytes were used for experiments within 10–14 days after the induction of differentiation. The RAW264.7 macrophage cell line was maintained in Dulbecco's modified Eagle's medium supplemented with 10% FBS and antibiotics. MeT-5A, a human mesothelial cell line immortalized through transfection with the pRSV-T plasmid (an SV40 ori-construct containing the SV40 early region and the Rous sarcoma virus long terminal repeat), was maintained in M199 medium supplemented with 10% FBS, 10 ng/ml epidermal growth factor, 870 nM insulin, 400 nM hydrocortisone, 0.3% (vol/vol) trace element B and antibiotics. Y-MESO-8A and Y-MESO-8D cell lines were maintained in RPMI 1640 medium supplemented with 10% FBS and antibiotics. All the cells were cultured in a humidified incubator with 5% CO_2 at 37°C.

Experimental animals

For animal experiments, 8-week-old male ddY mice (Japan SLC, Hamamatsu, Shizuoka, Japan) were used. The animals were housed in a specific pathogen-free animal facility with 12 h light/12 h dark cycle and allowed free access to food (CE-2, CLEA Japan, Tokyo, Japan) and water. These mice were subjected to a single intraperitoneal injection of 2.5 mg of asbestos fibers and killed after 3 days via cervical dislocation. Physiological saline (0.9%) was injected as a control. After killing, the epididymal fat pad was harvested; half of it was fixed in 10% phosphate-buffered formalin for histological analysis, whereas the other half was snap-frozen in liquid nitrogen and kept at −80°C until further use. The animal experiment was approved by the Animal Experiment Committee of the Nagoya University Graduate School of Medicine.

Oil Red O staining of adipocytes

Adipocyte maturation from the preadipocyte cell line was confirmed by staining the lipid droplets that accumulated in the cytoplasm of adipocytes during maturation using the Oil Red O staining method. After washing the mature adipocytes with phosphate-buffered saline, the cells were fixed with 10% phosphate-buffered formalin for 2 h. After another washing step, Oil Red O solution was added, and the cells were incubated at 37°C for 5 min. Images were acquired using a Nikon Eclipse TS-100 microscope (Nikon, Tokyo, Japan).

Fiber uptake by adipocytes

The uptake of asbestos fibers by adipocytes was analyzed by both light microscopy and transmission electron microscopy. Cultured adipocytes were exposed to 10 μg/cm^2 of asbestos fibers, and 24 h later, the cells were harvested by trypsinization and centrifuged to generate a cell pellet. For light microscopy, cell block was prepared by fixing the cells with 10% phosphate-buffered formalin and subsequently processed into a paraffin-embedded cell block. Sections of 4 μm were stained with Kernechtrot staining and viewed under ×100 magnification using a BZ-9000 microscope (Keyence, Osaka, Japan) to detect fibers inside the cells. For electron microscopy, cells were fixed with phosphate buffer containing 2.5% glutaraldehyde and 2% paraformaldehyde, followed by fixation with 1% osmium tetroxide. The cells were then embedded in Epon resin and cut into 80 nm ultrathin sections with diamond knife. After staining with uranyl acetate and lead citrate, detection of fibers inside the cells was performed using JEM-1400EX transmission electron microscope (JEOL, Tokyo, Japan).

Cell viability assay

The cytotoxicity of asbestos fibers on adipocytes, MeT-5A and RAW264.7 macrophages was measured using a CellTiter-Glo Luminescent Cell Viability Assay (Promega, Madison, WI). Asbestos fibers were added to the cells at a concentration of 10 μg/cm^2. After 72 h of incubation, the number of viable cells was evaluated via the addition of the CellTiter-Glo Luminescent Cell Viability Assay reagent followed by chemiluminescence measurement using a PowerScan4 plate reader (DS Pharma Biomedical, Osaka, Japan).

Microarray-based gene expression analysis

Microarray analysis was performed using an Agilent SurePrint G3 Mouse GE 8x60K Microarray slide and Agilent's Low Input Quick Amp Labeling Kit (Agilent Technologies, Santa Clara, CA) according to Agilent's One-Color Microarray-Based Gene Expression Analysis protocol. In total, 200 ng of total RNA extracted from adipocytes exposed to asbestos fibers under the conditions stated above was used as the initial material. Amplified cRNA was labeled with Cy3-CTP. Hybridization was performed by placing the slide in a hybridization oven equipped with a rotator and set at 65°C for 17 h. After hybridization, the microarray slide was washed with GE Wash Buffer and scanned, and data were analyzed using GeneSpring GX 10.02.2 software (Agilent Technologies).

Quantitative real-time reverse transcription–PCR

Total RNA was isolated from the differentiated adipocyte cell line or adipose tissue using the RNeasy Lipid Tissue Mini Kit (Qiagen, Valencia, CA). Total RNA was then reversed transcribed into complementary DNA using the SuperScript III First-Strand Synthesis Kit (Invitrogen, Grand Island, NY). Gene expression levels were quantitatively measured using the Platinum SYBR Green qPCR SuperMix-UDG kit (Invitrogen) and analyzed with an Applied Biosystems Model 7300 Real Time PCR System (Applied Biosystems, Foster City, CA). The β-actin level was used to normalize the messenger RNA (mRNA) level of all genes examined. The primer sequences used were as follows: mouse IL-6, forward, 5′-CTTCTTGGGACTGATGCTGG-3′, reverse, 5′-CAGAATTGCCATTGCACAAC-3′ (product size 185 bp); mouse β-actin, forward, 5′-ACATCCCCCAAAGTTCTACAAA-3′, reverse, 5′-TGAGGGACTTCCTGTAACCACT-3′ (product size 132 bp); mouse adiponectin, forward, 5′-GCAGGCATCCCAGGACATCC-3′, reverse, 5′-TCCTTTCCTGCCAGGGGTTC-3′ (product size 186 bp); mouse MCP-1, forward, 5′-CAGTTAACGCCCCACTCACC-3′, reverse, 5′-TCCTTCTTGG GGTCAGCACA-3′ (product size 163 bp); mouse prolactin family 2, subfamily c, member 5 (Prl2c5), forward, 5′-AACAAGGAACAAGCCAGGCACA-3′, reverse, 5′-ACCCCGTTCTGGACTGCGTT-3′ (product size 188 bp); mouse leptin, forward, 5′-CCAGCAGCTGCAAGGTGCAAGA-3′, reverse, 5′-CCCTCTGCTTGGCGGATACCGA-3′ (product size 214 bp) and mouse PAI-1, forward, 5′-ATGTGCACCTCTCCGCCCTCA-3′, reverse, 5′-GCTGCTCTTGGTCGGAAAGACTTG-3′ (product size 213 bp).

MCP-1 enzyme-linked immunosorbent assay

Differentiated adipocytes in a 6-well plate were exposed to different types of asbestos fibers and NT-tngl at 10 μg/cm^2 for 72 h. The cell culture medium was then collected, and the concentration of MCP-1 secreted by adipocytes into the culture medium was measured using the Quantikine Mouse JE/MCP-1 Immunoassay Kit (R&D Systems, Minneapolis, MN). The immunoassay was performed according to the manufacturer's instructions.

Immunohistochemistry

Paraffin-embedded tissue sections were deparaffinized and rehydrated. Antigen retrieval was performed by heating the sections with microwave using 10 mM citrate buffer, pH 6.0. Endogenous peroxidase was inhibited by incubating the sections with 0.3% hydrogen peroxide in methanol for 30 min. Tissue sections were then blocked with normal goat serum and incubated with rabbit polyclonal primary antibody against mouse MCP-1 (ab7202, abcam, Tokyo, Japan) or IL-6 (ab6672; abcam). After washing with phosphate-buffered saline, sections were incubated with biotinylated goat anti-rabbit immunoglobulin G secondary antibody. Detection of antigen–antibody complexes was performed by incubating the sections with horseradish peroxidase-conjugated streptavidin followed by 3,3′-diaminobenzidine. Images were acquired using BZ 9000 microscope.

Measurement of adipocyte size

Images of epididymal adipose tissue sections were acquired using BZ 9000 microscope at ×40 magnification. Ten random fields were taken for each section from five animals per group. Cell surface area was measured using ImageJ software (NIH, Bethesda, MD).

Transwell migration assay

Cell culture inserts and 24-well companion tissue culture plates from BD Falcon (Franklin Lakes, NJ) were used for transwell migration assay. The

cell culture insert contains a porous membrane with an 8 μm pore size. RAW264.7 macrophages were seeded into the insert at a density of 2×10^5 cells/insert. Conditioned medium collected from adipocytes that were treated or untreated with asbestos fibers was added to the lower chamber of the 24-well tissue culture plate. The plate was incubated for 24 h, followed by staining of the migrated cells with May–Grunwald's and Giemsa stains. Images were acquired in 10 random fields, and the number of migrated cells was counted.

MTT cell proliferation assay

MeT-5A cells were seeded into a 96-well tissue culture plate at a density of 5×10^3 cells/well. These cells were serum starved for 24 h before being treated with recombinant human MCP-1 at a concentration of 100 and 500 ng/ml. After 72 h of treatment, cell proliferation was measured using MTT. The MTT compound was dissolved in phosphate-buffered saline at a concentration of 5 mg/ml, and 20 μl was then added to each well. Cells were incubated with MTT for 4 h to allow the reduction of MTT into purple formazan. Culture

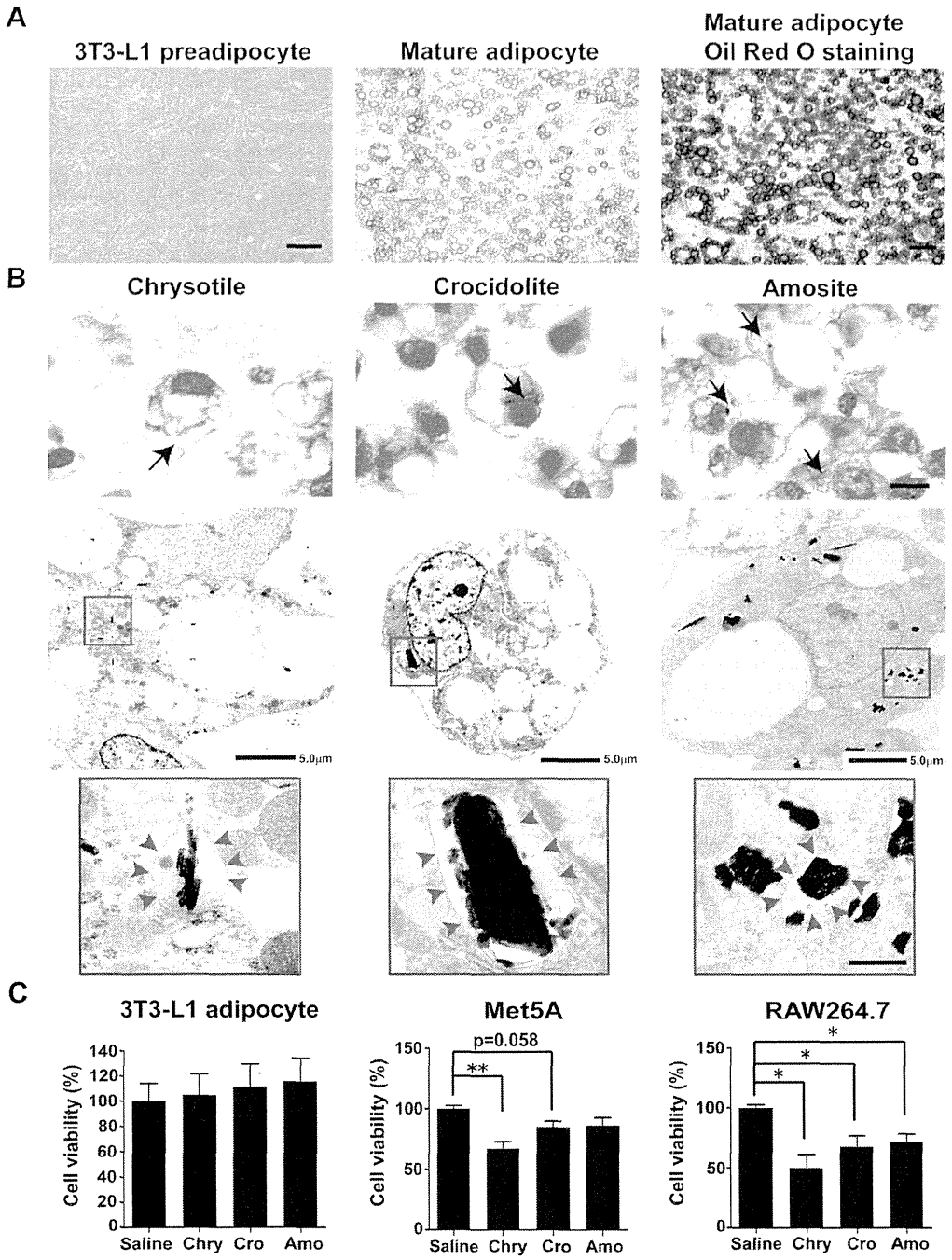

Fig. 1. Cultured adipocytes take up asbestos fibers but are resistant to their cytotoxic effect. (**A**) The 3T3-L1 preadipocyte cell line (left panel) was differentiated into mature adipocytes (middle panel) according to the standard differentiation protocol. Lipid droplets that accumulated in the mature adipocytes were stained by Oil Red O staining (right panel). Scale bars: left panel, 100 μm; middle and right panels, 20 μm. (**B**) The presence of asbestos fibers inside adipocytes was detected using light microscopy at ×100 magnification (upper panel) and transmission electron microscopy (middle and lower panels). Scale bars: upper panel, 10 μm; middle panel, 5 μm; lower panel, 500 nm. (**C**) The cytotoxicity of asbestos fibers on adipocytes, MeT-5A mesothelial cells and RAW264.7 macrophages was measured by the adenosine triphosphate cell viability assay. All the cells were exposed to 10 μg/cm^2 of asbestos fibers for 72 h. The results are shown as the mean ± SEM of three independent experiments. *$P \leq 0.05$, **$P \leq 0.005$. Amo, amosite; Chry, chrysotile; Cro, crocidolite.

medium containing MTT was then aspirated from the wells, followed by the addition of 100 μl of dimethyl sulfoxide into each well to dissolve the purple formazan crystals. The optical density was measured using a PowerScan4 plate reader.

Wound-healing assay

MeT-5A, Y-MESO-8A or Y-MESO-8D cells were grown in a 6-well tissue culture plate until the cells formed a confluent monolayer. A scratch was then made across the cell monolayer using a pipette tip. Recombinant human MCP-1 was added to some of the wells at a concentration of 500 ng/ml. Images of the wound were taken immediately after the scratch (designated as 0 h) and at 18, 24 and 48 h after the scratch. The width of the wound was measured using ImageJ software, and the percentage of wound healing was then calculated.

Statistical analysis

The statistical significance between two groups of interest was analyzed using the unpaired Student's *t*-test. A P value of <0.05 was considered significant.

Table I. Top 20 genes upregulated in asbestos-treated cultured adipocytes

Gene name	Accession number	Fold change
Top 20 genes upregulated in chrysotile-treated adipocytes		
Prolactin family 2, subfamily c, member 5 (Prl2c5)	NM_181852	18.596165
Fibrinogen-like protein-1 (Fgl1)	BC029734	8.48526
Chemokine (C-C motif) ligand 2 (Ccl2)	NM_011333	8.051252
Troponin T2, cardiac (Tnnt2), transcript variant 9	NM_011619	6.9297132
Prolactin family 2, subfamily c, member 1 (Prl2c1)	NM_001045532	6.292936
Secreted phosphoprotein 1 (Spp1)	NM_009263	5.334665
High-mobility group AT-hook 2 (Hmga2)	NM_010441	5.1633744
Chemokine (C-C motif) ligand 8 (Ccl8)	NM_021443	4.867768
lincRNA:chr19:9060613-9060851 forward strand		4.497705
Fos-like antigen 1 (Fosl1)	NM_010235	4.422233
Interleukin 1 receptor-like 1 (Il1rl1), transcript variant 1	NM_001025602	4.192457
Tumor necrosis factor receptor superfamily, member 9 (Tnfrsf9), transcript variant 1	NM_011612	4.0868807
Plasminogen activator, urokinase (Plau)	NM_008873	4.038391
Runt-related transcription factor 1 (Runx1), transcript variant 2	NM_001111022	3.8444314
Interleukin 1 receptor-like 1 (Il1rl1), transcript variant 2	NM_010743	3.7691207
cDNA sequence BC023744 (BC023744)	NM_001033311	3.6094844
Matrix metallopeptidase 10 (Mmp10)	NM_019471	3.6034727
Matrix metallopeptidase 13 (Mmp13)	NM_008607	3.5614529
Serine/threonine/tyrosine kinase 1 (Styk1)	NM_172891	3.4867864
Acyl-CoA synthetase bubblegum family member 1 (Acsbg1)	NM_053178	3.3379452
Top 20 genes upregulated in crocidolite-treated adipocytes		
Serum amyloid A 3 (Saa3)	NM_011315	21.692352
Haptoglobin (Hp)	NM_017370	11.54753
Dermokine (Dmkn), transcript variant 3	NM_001166173	9.095255
Suprabasin (Sbsn), transcript variant 1	NM_172205	7.677543
Secretory leukocyte peptidase inhibitor (Slpi)	NM_011414	6.6974707
Serine (or cysteine) peptidase inhibitor, clade A, member 3G (Serpina3g)	NM_009251	6.258521
PREDICTED: *Mus musculus* predicted gene, EG628900 (EG628900)	XM_893705	6.231637
Chemokine (C-C motif) ligand 2 (Ccl2)	NM_011333	5.961754
Chemokine (C-C motif) ligand 9 (Ccl9)	NM_011338	5.94364
Chitinase 3-like 1 (Chi3l1)	NM_007695	5.8167386
Lipocalin-2 (Lcn2)	NM_008491	5.732993
Chemokine (C-X-C motif) receptor 7 (Cxcr7)	NM_007722	5.6649795
Prolactin family 2, subfamily c, member 5 (Prl2c5)	NM_181852	5.511816
Complement component 4B (Childo blood group) (C4b)	NM_009780	5.504423
Serine (or cysteine) peptidase inhibitor, clade A, member 3H (Serpina3h)	NM_001034870	5.3198853
Runt-related transcription factor 1 (Runx1), transcript variant 4	NM_009821	5.090166
Triggering receptor expressed on myeloid cells 2 (Trem2)	NM_031254	4.8963866
Fibrinogen-like protein 1 (Fgl1)	NM_145594	4.8214192
Cannabinoid receptor 1 (brain) (Cnr1)	NM_007726	4.818088
Placental protein 11 related (Pp11r), transcript variant 2	NM_001168693	4.759451
Top 12 genes upregulated in amosite-treated adipocytes		
Extended synaptotagmin-like protein 3 (Esyt3)	NM_177775	2.988655
Budding uninhibited by benzimidazoles 1 homolog (*Saccharomyces cerevisiae*) (Bub1)	NM_009772	2.4976056
Potassium inwardly rectifying channel, subfamily J, member 6 (Kcnj6)	NM_001025585	2.4706264
lincRNA:chr4:21683562-21694344 reverse strand		2.4663801
PREDICTED: *M.musculus* predicted gene, EG666955 (EG666955)	XM_001000153	2.3627758
lincRNA:chr2:75493715-75494227 reverse strand		2.3625197
Adult male tongue cDNA, RIKEN full-length enriched library, clone:2310006M14 product:hypothetical protein, full insert sequence	AK009188	2.271196
ATPase, Ca^{++} transporting, type 2C, member 2 (Atp2c2)	NM_026922	2.2707396
lincRNA:chr6:31017987-31174287 reverse strand		2.2265513
Adult male olfactory brain cDNA, RIKEN full-length enriched library, clone:6430601O08 product:similar to Pol protein (fragment) (*M.musculus*), full insert sequence	AK032580	2.2096734
lincRNA:chr19:59498190-59531390 reverse strand		2.1915858
lincRNA:chr17:27479404-27481770 forward strand		2.082444

ATPase, adenosine triphosphatase; cDNA, complementary DNA. Twelve genes with >2-fold change were selected for amosite.

Results

Uptake of asbestos fibers by cultured adipocytes

The 3T3-L1 preadipocyte cell line was used to generate mature adipocytes according to the standard differentiation protocol. Adipocytes were used for subsequent experiments 10–14 days after the initiation of differentiation. During differentiation, the adipocytes accumulated lipid droplets in the cytoplasm that stained red upon Oil Red O staining (Figure 1A). Three different types of asbestos fibers, chrysotile, crocidolite and amosite fibers, were added to the adipocytes, followed by the assessment of fiber uptake using a cell block and light microscopy. Fiber uptake by the adipocytes was observed for all the asbestos types (Figure 1B, upper panel). Our findings were further supported by transmission electron microscopy, which clearly demonstrated fiber internalization by adipocytes (Figure 1B, lower panel). High magnification revealed the structure of a vesicular membrane around the asbestos fibers.

Asbestos fibers induce cell death when administered to mesothelial cells and macrophages (7,29). We compared the cytotoxicity of asbestos fibers on the cultured adipocytes, MeT-5A mesothelial cells and RAW264.7 macrophages by exposing them to the same concentration of asbestos fibers (10 μg/cm^2). When we performed an adenosine triphosphate detection cell viability assay on these different cell types, we did not observe any cytotoxic effect of asbestos fibers on the adipocytes, which was in contrast to mesothelial cells and macrophages (Figure 1C).

Cultured adipocytes showed changes in gene expression after asbestos exposure

As noted above, we hypothesized that the endocrine function of adipose tissue is potentially affected by asbestos exposure. To screen for genes with altered expression in asbestos-exposed adipocytes, we performed microarray gene expression analysis on the total RNA isolated from adipocytes after 72 h of exposure to asbestos fibers (GEO accession no.: GSE42330). The microarray results are shown in Table I. The top 20 genes that were upregulated in adipocytes after exposure to the different types of asbestos fibers are listed. More information can be found in the Supplementary Tables 1–3, available at *Carcinogenesis* Online. Gene expression analysis revealed the upregulation of some inflammation-related genes in adipocytes following exposure to asbestos fibers, including serum amyloid A3, haptoglobin and urokinase-type plasminogen activator. More importantly, we found the upregulation of an important adipocytokine that is commonly reported to be upregulated in obesity and is responsible for the related chronic inflammation and associated metabolic complications: chemokine C-C motif ligand 2 (Ccl2), which is also known as MCP-1. Other members of the C-C motif chemokine family were also upregulated, such as Ccl6, Ccl8 and Ccl9. Another gene that was upregulated in both chrysotile- and crocidolite-treated adipocytes was Prl2c5, which belongs to the prolactin superfamily.

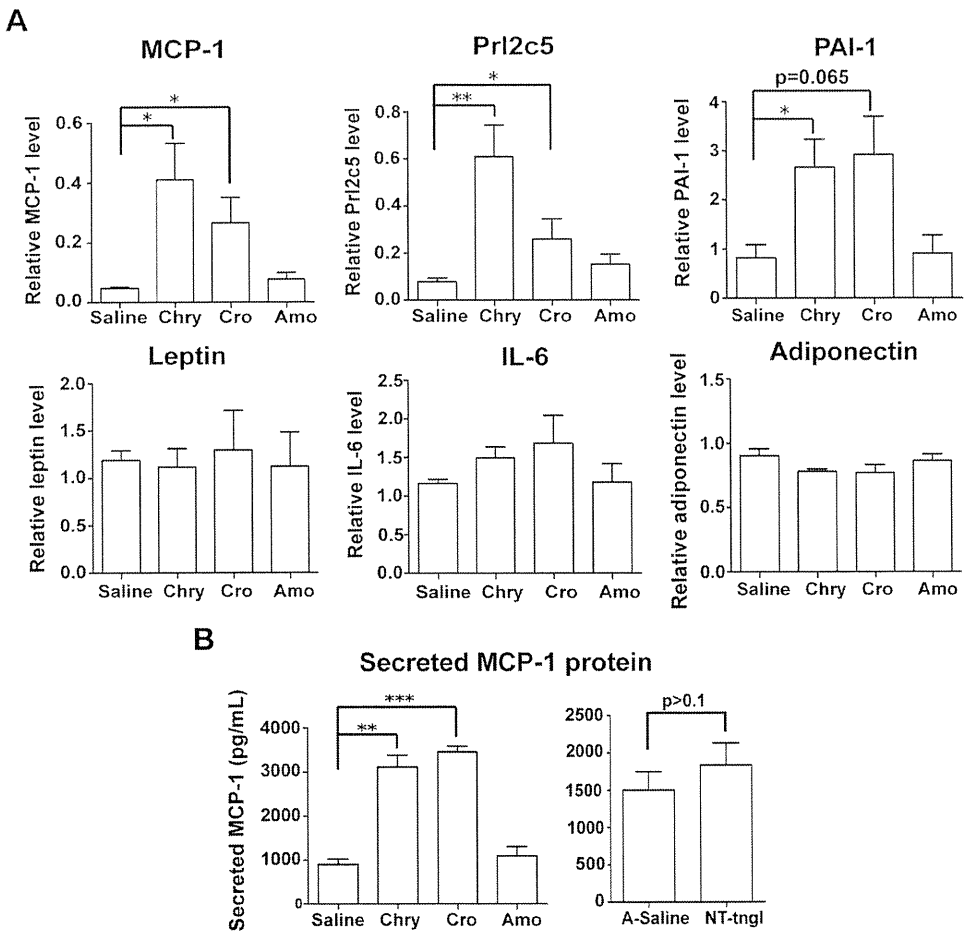

Fig. 2. Alterations in the expression level of adipocytokines in cultured adipocytes after asbestos exposure. Cultured adipocytes were exposed to chrysotile, crocidolite or amosite fibers at 10 μg/cm^2 for 72 h, with physiological saline as the control. (**A**) The gene expression level of various adipocytokines was measured by quantitative real-time RT–PCR and is shown relative to that of β-actin. (**B**) The secretion of MCP-1 into culture medium was measured by an MCP-1 immunoassay. In addition to asbestos fibers, adipocytes were also exposed to NT-tngl under the same experimental condition. The results are shown as the mean ± SEM of three independent experiments, *$P \leq 0.05$, **$P \leq 0.005$, ***$P \leq 0.001$. Amo, amosite; A-Saline, saline containing 0.5% bovine serum albumin; Chry, chrysotile; Cro, crocidolite.

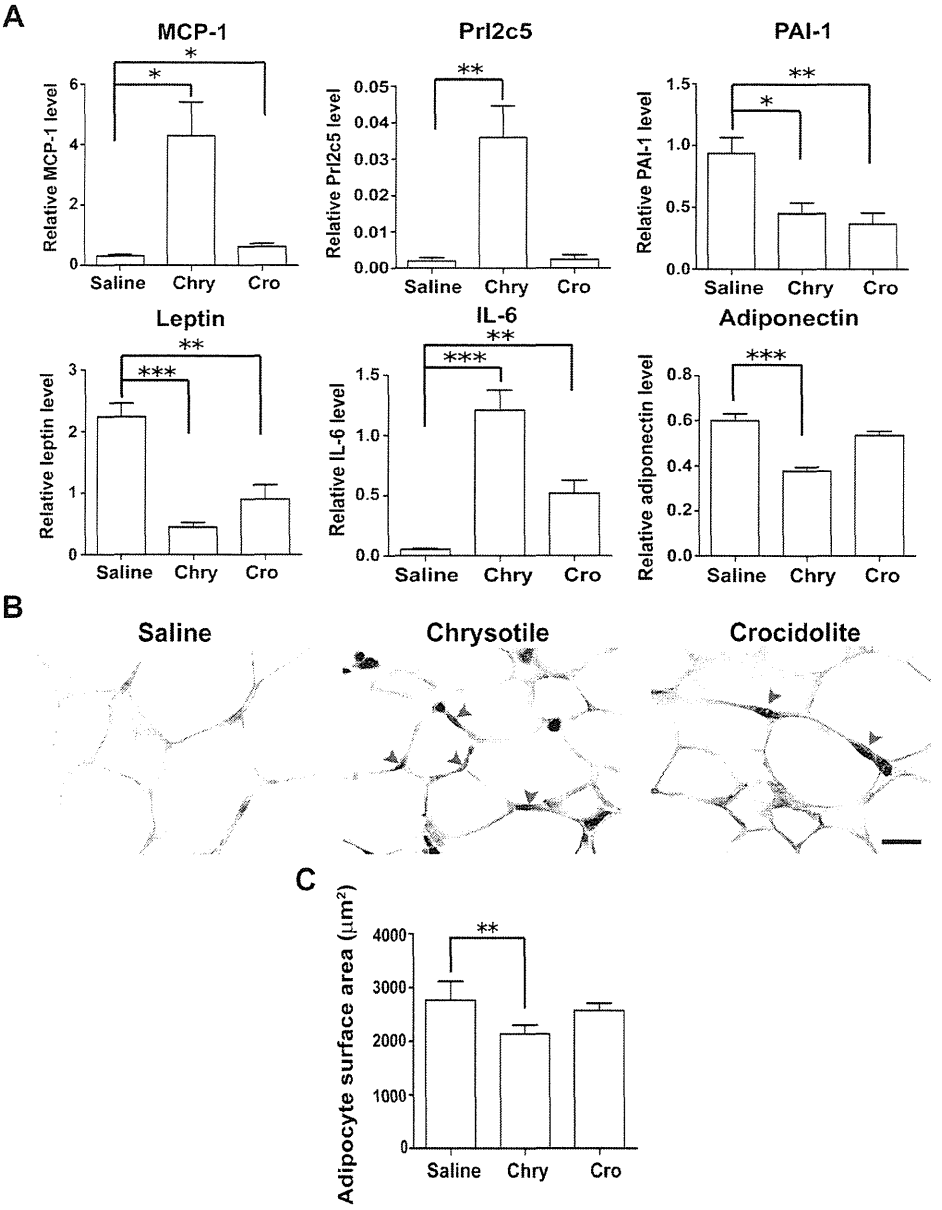

Fig. 3. Adipose tissues of mice injected with asbestos fibers show changes in adipocytokine expression levels. A total of 2.5 mg of chrysotile or crocidolite fibers was injected into the peritoneal cavity of mice, with physiological saline used as a control. Epididymal adipose tissue was harvested after 3 days. (**A**) The gene expression level of various adipocytokines in the epididymal adipose tissue was measured by quantitative real-time RT–PCR. The results are shown as the mean ± SEM (n = 6 per group). (**B**) Representative images of epididymal adipose tissue immunostained for MCP-1 expression. Scale bar: 20 μm. (**C**) Measurement of adipocyte cell surface area from adipose tissue sections using image analyzing software (n = 5 per group). *$P \leq 0.05$, **$P \leq 0.005$, ***$P \leq 0.001$. Chry, chrysotile; Cro, crocidolite.

MCP-1 was increased at the mRNA and protein level in adipocytes treated with asbestos fibers

Quantitative real-time reverse transcription–PCR (RT–PCR) was performed to evaluate the expression level of MCP-1, Prl2c5 and several other commonly known adipocytokines (PAI-1, leptin, IL-6 and adiponectin) in asbestos-treated or untreated adipocytes. In support of the microarray results, quantitative real-time RT–PCR showed the increased mRNA expression of MCP-1 and Prl2c5 in adipocytes following asbestos exposure (Figure 2A). Regarding the other adipocytokines examined, PAI-1 was also upregulated, whereas leptin, IL-6 and adiponectin did not show any significant alterations. Nevertheless, a slight decrease in adiponectin mRNA expression was observed. An enzyme-linked immunosorbent assay was performed to measure the secretion of MCP-1 protein into the culture medium of adipocytes treated with asbestos fibers. The enzyme-linked immunosorbent assay results corroborated those of quantitative real-time RT–PCR, showing a significant elevation of MCP-1 secretion by adipocytes treated with chrysotile and crocidolite fibers (control = 900.7 pg/ml, chrysotile treated = 3116.5 pg/ml, crocidolite treated = 3455.9 pg/ml, $P \leq 0.005$) (Figure 2B, left panel). Amosite-treated adipocytes did not show any apparent change in MCP-1 expression at either the mRNA or protein level. To determine whether any type of particulate is able to induce the same response, we also exposed the adipocytes to NT-tngl. Exposure to NT-tngl did not induce any significant increase in MCP-1 secretion from the adipocytes (Figure 2B, right panel).

Asbestos fibers dysregulated adipocytokine levels in adipose tissue of asbestos-exposed mice

To determine whether adipose tissue in living animals also responds to asbestos exposure, we injected chrysotile or crocidolite fibers into the peritoneal cavity of mice, with physiological saline as a control. Epididymal fat pads were harvested after 3 days, followed by quantitative real-time RT–PCR to examine changes in the expression level of adipocytokines. Again, the mRNA levels of MCP-1 and Prl2c5 were both upregulated in the adipose tissue of mice injected with asbestos fibers (Figure 3A). Regarding adiponectin, its suppressed expression level in the adipose tissue was more apparent than in the cultured adipocytes and was significant in chrysotile-injected mice. Leptin and IL-6 were significantly downregulated and upregulated, respectively, although no significant change in these two genes was observed in cultured adipocytes (Figure 2A). PAI-1 was the only exception that showed contradictory results between *in vitro* and *in vivo* assays. Immunohistochemical staining for MCP-1 and IL-6 was also performed on the adipose tissue sections. We found that in both chrysotile and crocidolite-injected mice, there was more intense MCP-1 staining in the cytoplasm of adipocytes compared with the saline-injected mice (Figure 3B). In contrast, the adipocytes did not show apparent positive staining of IL-6 (Supplementary Figure 1, available at *Carcinogenesis* Online), indicating that other inflammatory cells might be responsible for IL-6 mRNA upregulation as shown in Figure 3A. We have also noted some changes in adipocyte size and measurement of adipocyte surface area revealed a reduction of adipocyte size in asbestos-injected mice (Figure 3C).

MCP-1 promoted cancer cell phenotypes of mesothelial cells

Based on the well-known effect of MCP-1 as a macrophage chemoattractant, the increased secretion of MCP-1 by adipocytes in response to asbestos fibers might implicate an important indirect role of adipose tissue in enhancing the recruitment of macrophages to the sites of asbestos deposition. We collected culture media from asbestos-treated adipocytes and examined the ability of these conditioned media to induce macrophage migration. The transwell migration assay results revealed an increase in macrophage migration in response to the conditioned media from asbestos-treated adipocytes, which was most probably mediated by increased MCP-1 secretion (Figure 4).

Many chemokines have been reported to exert a mitogenic effect and are thus able to promote cancer development. We studied the effect of MCP-1 on mesothelial cell proliferation by treating MeT-5A cells with recombinant MCP-1 protein. MCP-1 showed a marginal but not significant effect on mesothelial cell proliferation (Figure 5A). In addition, we assayed the effect of MCP-1 on mesothelial cell migration. A wound-healing assay was performed in MeT-5A cells in the presence or absence of recombinant MCP-1 protein. We did not observe any effect of MCP-1 on MeT-5A cell migration (Figure 5B, left panel). However, we found that MCP-1 promoted the migration of the human mesothelioma cells Y-MESO-8A and Y-MESO-8D (Figure 5B, middle and right panels).

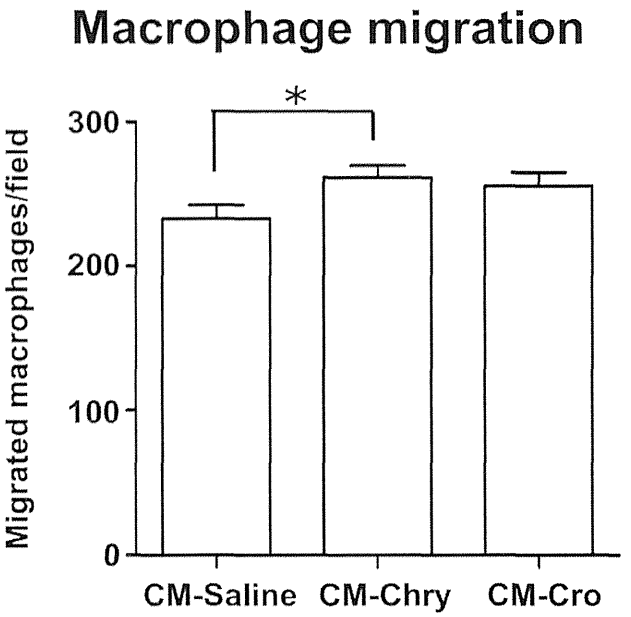

Fig. 4. Adipocytes induce increased macrophage migration following asbestos exposure. Cultured adipocytes were exposed to chrysotile or crocidolite fibers at 10 μg/cm^2 for 72 h, with physiological saline as a control. Conditioned medium was collected and assayed with a transwell migration assay to determine the ability of the conditioned media to induce macrophage migration. The results are shown as the mean ± SEM of three independent experiments. *$P \leq 0.05$. Chry, chrysotile; CM, conditioned medium; Cro, crocidolite.

Discussion

Our results revealed for the first time that asbestos fibers are able to directly affect the endocrine activity of adipocytes. This effect might be mediated through a direct interaction, as we showed that adipocytes were able to phagocytose asbestos fibers. Although adipose tissue is more abundant in the peritoneal cavity, it is also present in the pleural cavity, e.g. submesothelial space of the parietal pleura, around the pericardial sac and near the mediastinum (30,31). These anatomic locations render relevance of adipose tissue as it is accessible for the inhaled fibers through fiber translocation. In response to asbestos exposure, adipocytes upregulated proinflammatory adipocytokine such as MCP-1 but suppressed the level of anti-inflammatory adipocytokine, adiponectin, thereby shifting the balance towards a proinflammatory condition. Increased MCP-1 secretion by adipocytes might result in enhanced macrophage recruitment which in turn elaborates various cytokines and chemokines, leading to a vicious cycle that aggravates inflammation. Our results using adipocyte conditioned media to induce macrophage migration supported this notion. The role of adipose tissue in asbestos-induced inflammation can thus be both direct and indirect. MCP-1 has been reported to induce the proliferation of primary human pleural mesothelial cells (32) and our results using MeT-5A are consistent with the report. We also showed that MCP-1 promoted the migration of human mesothelioma cells. In addition, we observed a reduction in adipocyte size in asbestos-injected mice, which is probably due to the more active state of the adipocytes that requires higher metabolic rate.

MCP-1 transgenic and MCP-1$^{-/-}$ mice have previously been generated and characterized. MCP-1 overexpression in specific organs resulted in the enhanced recruitment of blood monocytes into the parenchyma of these organs (33,34). In contrast, in MCP$^{-/-}$ mice, there is a reduction in mononuclear cell infiltrate when these mice are challenged with different inflammatory stimuli (35). These mouse models are often used in studies related to obesity and insulin resistance. Kanda *et al.* (24) generated adipose-specific MCP-1 transgenic mice characterized by insulin resistance, hepatic steatosis and a higher degree of macrophage infiltration into adipose tissue. These MCP-1 genetically engineered mice might be a useful tool in our further studies to establish an association between MCP-1 expression and asbestos-induced mesotheliomagenesis.

In this study, we primarily focused on the possible tumor-promoting effects of MCP-1. Other adipocytokines with dysregulated expression might also play a cancer-promoting role. For instance, adiponectin expression is inversely correlated with human cancers. Low circulating levels of adiponectin have been associated with an increased risk of several cancers, such as colorectal cancer (36), endometrial cancer (37), postmenopausal breast cancer (38), gastric cancer (39) and prostate cancer (40). Adiponectin was reported to be able to inhibit the transcription factor nuclear factor-κB (41,42), which is

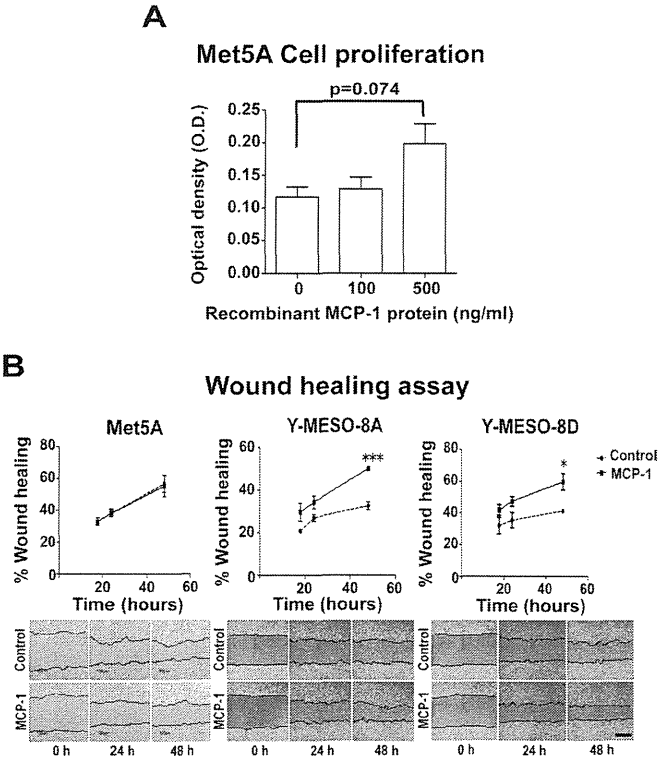

Fig. 5. Cancer-promoting effects of MCP-1. (**A**) Recombinant MCP-1 protein stimulates cell proliferation of the human mesothelial cell line MeT-5A, as measured by the MTT cell proliferation assay. (**B**) Recombinant MCP-1 protein induces the migration of the human mesothelioma cells Y-MESO-8A and Y-MESO-8D, as measured by the wound-healing assay. The results are shown as the mean ± SEM of three independent experiments. $^{*}P \leq 0.05$, $^{***}P \leq 0.001$.

a key molecule activated by asbestos fibers in mesothelial cells and macrophages that is responsible for inflammation. Our results suggested that asbestos fibers can cause a downregulation of adiponectin. The exact roles of leptin and PAI-1 in inflammation are still not entirely clear, although both were shown to be upregulated in obesity-related inflammation (43–45). A member of the prolactin superfamily, Prl2c5, was also upregulated. Current information regarding Prl2c5 is still relatively scarce, but this protein most probably shares many characteristics of prolactin, which is known to possess mitogenic property (46). Prolactin was newly found as an adipocytokine secreted by human adipose tissue (47,48). Several other genes more recently characterized as adipokines were also upregulated. Some of these genes, such as haptoglobin and lipocalin-2, bind to iron and can thus contribute to iron overload, which was shown to play an important role in asbestos-induced mesothelioma development (49). Another interesting upregulated peptide was secreted phosphoprotein 1, also known as osteopontin. Mesothelioma patients often have increased serum osteopontin levels and it was suggested to be a useful biomarker for the early diagnosis of mesothelioma (50). More detailed studies are needed to fully elucidate the potential pathogenic roles of these various dysregulated adipocytokines in mesothelial carcinogenesis. Moreover, a long-term study is needed to assess whether these alterations observed are long-term effects.

Interestingly, we found that chrysotile fibers appeared to be the most inflammogenic. Our results showed that chrysotile fibers dysregulated various adipocytokine levels to a higher extent than crocidolite and amosite fibers. This finding corroborates our recently published data that chrysotile fibers induced a significantly earlier development of malignant mesothelioma with intraperitoneal injection in rats compared with crocidolite and amosite fibers (49). The relatively stronger carcinogenicity of chrysotile fibers might be linked to a higher degree of adipose tissue inflammation. The reason underlying why chrysotile fibers seem to have a stronger inflammogenic effect on adipocytes is still not known, although our results showed that all types of asbestos fibers were internalized by the adipocytes.

To our knowledge, this is the first report of a potential association between dysregulated adipose endocrine function and asbestos-induced mesothelial carcinogenesis. We have shown that asbestos fibers are able to directly trigger an inflammatory response in adipocytes by dysregulating adipocytokine production. These adipocytokines might act locally to stimulate the growth/migration/survival of mesothelial cells and thus promote the development of malignant mesothelioma. The modulation of these adipocytokines might represent a novel strategy to extend the lifespan of mesothelioma patients.

Supplementary material

Supplementary Tables 1–3 and Figure 1 can be found at http://carcin.oxfordjournals.org/

Funding

Princess Takamatsu Cancer Research Fund (10-24213); Ministry of Health, Labour and Welfare of Japan (25-A-5); Ministry of Education, Culture, Sports, Science and Technology of Japan (24390094). The funders had no role in study design, data collection and analysis, decision to publish or preparation of the manuscript.

Conflict of Interest Statement: None declared.

References

1. Wagner,J.C. *et al.* (1960) Diffuse pleural mesothelioma and asbestos exposure in the North Western Cape Province. *Br. J. Ind. Med.*, **17**, 260–271.
2. Davies,P. *et al.* (1974) Asbestos induces selective release of lysosomal enzymes from mononuclear phagocytes. *Nature*, **251**, 423–425.
3. Hamilton,J.A. (1980) Macrophage stimulation and the inflammatory response to asbestos. *Environ. Health Perspect.*, **34**, 69–74.
4. Choe,N. *et al.* (1997) Pleural macrophage recruitment and activation in asbestos-induced pleural injury. *Environ. Health Perspect.*, **105** (suppl. 5), 1257–1260.
5. Ramos-Nino,M.E. *et al.* (2002) Mesothelial cell transformation requires increased AP-1 binding activity and ERK-dependent Fra-1 expression. *Cancer Res.*, **62**, 6065–6069.
6. Swain,W.A. *et al.* (2004) Activation of p38 MAP kinase by asbestos in rat mesothelial cells is mediated by oxidative stress. *Am. J. Physiol. Lung Cell. Mol. Physiol.*, **286**, L859–L865.
7. Yang,H. *et al.* (2006) TNF-alpha inhibits asbestos-induced cytotoxicity via a NF-kappaB-dependent pathway, a possible mechanism for asbestos-induced oncogenesis. *Proc. Natl Acad. Sci. USA*, **103**, 10397–10402.
8. Jagadeeswaran,R. *et al.* (2006) Functional analysis of c-Met/hepatocyte growth factor pathway in malignant pleural mesothelioma. *Cancer Res.*, **66**, 352–361.
9. Yang,H. *et al.* (2010) Programmed necrosis induced by asbestos in human mesothelial cells causes high-mobility group box 1 protein release and resultant inflammation. *Proc. Natl Acad. Sci. USA*, **107**, 12611–12616.
10. Whitaker,D. *et al.* (1984) Cytologic and tissue culture characteristics of asbestos-induced mesothelioma in rats. *Acta Cytol.*, **28**, 185–189.
11. Suzuki,Y. *et al.* (1984) Malignant mesothelioma induced by asbestos and zeolite in the mouse peritoneal cavity. *Environ. Res.*, **35**, 277–292.
12. Toyokuni,S. (2009) Mechanisms of asbestos-induced carcinogenesis. *Nagoya J. Med. Sci.*, **71**, 1–10.
13. Bolton,R.E. *et al.* (1982) Variations in the carcinogenicity of mineral fibres. *Ann. Occup. Hyg.*, **26**, 569–582.
14. Carthew,P. *et al.* (1992) Intrapleural administration of fibres induces mesothelioma in rats in the same relative order of hazard as occurs in man after exposure. *Hum. Exp. Toxicol.*, **11**, 530–534.
15. Fantuzzi,G. (2005) Adipose tissue, adipokines, and inflammation. *J. Allergy Clin. Immunol.*, **115**, 911–9; quiz 920.
16. Greenberg,A.S. *et al.* (2006) Obesity and the role of adipose tissue in inflammation and metabolism. *Am. J. Clin. Nutr.*, **83**, 461S–465S.
17. Itoh,M. *et al.* (2011) Adipose tissue remodeling as homeostatic inflammation. *Int. J. Inflam.*, **2011**, 720926.

18. Bianchini,F. *et al.* (2002) Overweight, obesity, and cancer risk. *Lancet Oncol.*, **3**, 565–574.
19. Calle,E.E. *et al.* (2003) Overweight, obesity, and mortality from cancer in a prospectively studied cohort of U.S. adults. *N. Engl. J. Med.*, **348**, 1625–1638.
20. Reeves,G.K. *et al.* Million Women Study Collaboration. (2007) Cancer incidence and mortality in relation to body mass index in the Million Women Study: cohort study. *BMJ*, **335**, 1134.
21. Renehan,A.G. *et al.* (2008) Body-mass index and incidence of cancer: a systematic review and meta-analysis of prospective observational studies. *Lancet*, **371**, 569–578.
22. Hotamisligil,G.S. *et al.* (1993) Adipose expression of tumor necrosis factor-alpha: direct role in obesity-linked insulin resistance. *Science*, **259**, 87–91.
23. Sartipy,P. *et al.* (2003) Monocyte chemoattractant protein 1 in obesity and insulin resistance. *Proc. Natl Acad. Sci. USA*, **100**, 7265–7270.
24. Kanda,H. *et al.* (2006) MCP-1 contributes to macrophage infiltration into adipose tissue, insulin resistance, and hepatic steatosis in obesity. *J. Clin. Invest.*, **116**, 1494–1505.
25. van Kruijsdijk,R.C. *et al.* (2009) Obesity and cancer: the role of dysfunctional adipose tissue. *Cancer Epidemiol. Biomarkers Prev.*, **18**, 2569–2578.
26. Cousin,B. *et al.* (1999) A role for preadipocytes as macrophage-like cells. *FASEB J.*, **13**, 305–312.
27. Villena,J.A. *et al.* (2001) Adipose tissues display differential phagocytic and microbicidal activities depending on their localization. *Int. J. Obes. Relat. Metab. Disord.*, **25**, 1275–1280.
28. Usami,N. *et al.* (2006) Establishment and characterization of four malignant pleural mesothelioma cell lines from Japanese patients. *Cancer Sci.*, **97**, 387–394.
29. Nagai,H. *et al.* (2011) Diameter and rigidity of multiwalled carbon nanotubes are critical factors in mesothelial injury and carcinogenesis. *Proc. Natl Acad. Sci. USA*, **108**, E1330–E1338.
30. Okby,N.T. *et al.* (2000) Liposarcoma of the pleural cavity: clinical and pathologic features of 4 cases with a review of the literature. *Arch. Pathol. Lab. Med.*, **124**, 699–703.
31. Shen,W. *et al.* (2003) Adipose tissue quantification by imaging methods: a proposed classification. *Obes. Res.*, **11**, 5–16.
32. Nasreen,N. *et al.* (2000) MCP-1 in pleural injury: CCR2 mediates haptotaxis of pleural mesothelial cells. *Am. J. Physiol. Lung Cell. Mol. Physiol.*, **278**, L591–L598.
33. Fuentes,M.E. *et al.* (1995) Controlled recruitment of monocytes and macrophages to specific organs through transgenic expression of monocyte chemoattractant protein-1. *J. Immunol.*, **155**, 5769–5776.
34. Gunn,M.D. *et al.* (1997) Monocyte chemoattractant protein-1 is sufficient for the chemotaxis of monocytes and lymphocytes in transgenic mice but requires an additional stimulus for inflammatory activation. *J. Immunol.*, **158**, 376–383.
35. Lu,B. *et al.* (1998) Abnormalities in monocyte recruitment and cytokine expression in monocyte chemoattractant protein 1-deficient mice. *J. Exp. Med.*, **187**, 601–608.
36. Wei,E.K. *et al.* (2005) Low plasma adiponectin levels and risk of colorectal cancer in men: a prospective study. *J. Natl Cancer Inst.*, **97**, 1688–1694.
37. Dal Maso,L. *et al.* (2004) Circulating adiponectin and endometrial cancer risk. *J. Clin. Endocrinol. Metab.*, **89**, 1160–1163.
38. Mantzoros,C. *et al.* (2004) Adiponectin and breast cancer risk. *J. Clin. Endocrinol. Metab.*, **89**, 1102–1107.
39. Ishikawa,M. *et al.* (2005) Plasma adiponectin and gastric cancer. *Clin. Cancer Res.*, **11** (2 Pt 1), 466–472.
40. Goktas,S. *et al.* (2005) Prostate cancer and adiponectin. *Urology*, **65**, 1168–1172.
41. Ajuwon,K.M. *et al.* (2005) Adiponectin inhibits LPS-induced NF-kappaB activation and IL-6 production and increases PPARgamma2 expression in adipocytes. *Am. J. Physiol. Regul. Integr. Comp. Physiol.*, **288**, R1220–R1225.
42. Wulster-Radcliffe,M.C. *et al.* (2004) Adiponectin differentially regulates cytokines in porcine macrophages. *Biochem. Biophys. Res. Commun.*, **316**, 924–929.
43. Auwerx,J. *et al.* (1988) Tissue-type plasminogen activator antigen and plasminogen activator inhibitor in diabetes mellitus. *Arteriosclerosis*, **8**, 68–72.
44. Juhan-Vague,I. *et al.* (1989) Increased plasminogen activator inhibitor activity in non insulin dependent diabetic patients–relationship with plasma insulin. *Thromb. Haemost.*, **61**, 370–373.
45. Hauner,H. (2005) Secretory factors from human adipose tissue and their functional role. *Proc. Nutr. Soc.*, **64**, 163–169.
46. Welsch,C.W. *et al.* (1977) Prolactin and murine mammary tumorigenesis: a review. *Cancer Res.*, **37**, 951–963.
47. Zinger,M. *et al.* (2003) Prolactin expression and secretion by human breast glandular and adipose tissue explants. *J. Clin. Endocrinol. Metab.*, **88**, 689–696.
48. Hugo,E.R. *et al.* (2008) Prolactin release by adipose explants, primary adipocytes, and LS14 adipocytes. *J. Clin. Endocrinol. Metab.*, **93**, 4006–4012.
49. Jiang,L. *et al.* (2012) Iron overload signature in chrysotile-induced malignant mesothelioma. *J. Pathol.*, **228**, 366–377.
50. Pass,H.I. *et al.* (2005) Asbestos exposure, pleural mesothelioma, and serum osteopontin levels. *N. Engl. J. Med.*, **353**, 1564–1573.

Received December 5, 2012; revised June 25, 2013; accepted July 31, 2013

Published OnlineFirst January 27, 2014; DOI: 10.1158/2159-8290.CD-13-0633

RESEARCH BRIEF

CD74–NRG1 Fusions in Lung Adenocarcinoma

Lynnette Fernandez-Cuesta[1], Dennis Plenker[1], Hirotaka Osada[19], Ruping Sun[13], Roopika Menon[9,14], Frauke Leenders[1,3], Sandra Ortiz-Cuaran[1], Martin Peifer[1,5], Marc Bos[1], Juliane Daßler[15], Florian Malchers[1], Jakob Schöttle[1,10], Wenzel Vogel[14], Ilona Dahmen[1], Mirjam Koker[1], Roland T. Ullrich[2,10], Gavin M. Wright[21], Prudence A. Russell[22], Zoe Wainer[21], Benjamin Solomon[23], Elisabeth Brambilla[24], Hélène Nagy-Mignotte[25], Denis Moro-Sibilot[25], Christian G. Brambilla[25], Sylvie Lantuejoul[24], Janine Altmüller[6,7,12], Christian Becker[6], Peter Nürnberg[5,6,7], Johannes M. Heuckmann[9], Erich Stoelben[11], Iver Petersen[16], Joachim H. Clement[17], Jörg Sänger[18], Lucia A. Muscarella[26], Annamaria la Torre[26], Vito M. Fazio[26,27], Idoya Lahortiga[28], Timothy Perera[29], Souichi Ogata[29], Marc Parade[29], Dirk Brehmer[29], Martin Vingron[13], Lukas C. Heukamp[8], Reinhard Buettner[3,4,8], Thomas Zander[1,2,4], Jürgen Wolf[2,3,4], Sven Perner[14], Sascha Ansén[2], Stefan A. Haas[13], Yasushi Yatabe[20], and Roman K. Thomas[1,3,8]

ABSTRACT We discovered a novel somatic gene fusion, *CD74–NRG1*, by transcriptome sequencing of 25 lung adenocarcinomas of never smokers. By screening 102 lung adenocarcinomas negative for known oncogenic alterations, we found four additional fusion-positive tumors, all of which were of the invasive mucinous subtype. Mechanistically, CD74–NRG1 leads to extracellular expression of the EGF-like domain of NRG1 III-β3, thereby providing the ligand for ERBB2–ERBB3 receptor complexes. Accordingly, ERBB2 and ERBB3 expression was high in the index case, and expression of phospho-ERBB3 was specifically found in tumors bearing the fusion ($P < 0.0001$). Ectopic expression of CD74–NRG1 in lung cancer cell lines expressing ERBB2 and ERBB3 activated ERBB3 and the PI3K–AKT pathway, and led to increased colony formation in soft agar. Thus, *CD74–NRG1* gene fusions are activating genomic alterations in invasive mucinous adenocarcinomas and may offer a therapeutic opportunity for a lung tumor subtype with, so far, no effective treatment.

SIGNIFICANCE: *CD74–NRG1* fusions may represent a therapeutic opportunity for invasive mucinous lung adenocarcinomas, a tumor with no effective treatment that frequently presents with multifocal unresectable disease. *Cancer Discov; 4(4); 415–22. ©2014 AACR.*

Authors' Affiliations: [1]Department of Translational Genomics; [2]Department I of Internal Medicine; [3]Laboratory of Translational Cancer Genomics; [4]Network Genomic Medicine, University Hospital Cologne, Center of Integrated Oncology Cologne-Bonn; [5]Center for Molecular Medicine Cologne (CMMC); [6]Cologne Center for Genomics (CCG); [7]Cologne Excellence Cluster on Cellular Stress Responses in Aging-Associated Diseases (CECAD); [8]Department of Pathology, University Hospital Medical Center, University of Cologne; [9]Blackfield AG; [10]Max Planck Institute for Neurological Research; [11]Thoracic Surgery, Lungenklinik Merheim, Kliniken der Stadt Köln gGmbH; [12]Institute of Human Genetics, Cologne; [13]Computational Molecular Biology Department, Max Planck Institute for Molecular Genetics, Berlin; [14]Department of Prostate Cancer Research, Institute of Pathology; [15]Institute for Clinical Chemistry and Clinical Pharmacology, University Hospital Bonn, Bonn; [16]Institute of Pathology; [17]Department of Internal Medicine II, Jena University Hospital, Friedrich-Schiller-University, Jena; [18]Institute for Pathology Bad Berka, Bad Berka, Germany; [19]Division of Molecular Oncology, Aichi Cancer Center Research Institute; [20]Department of Pathology and Molecular Diagnostics, Aichi Cancer Center, Nagoya, Japan; Departments of [21]Surgery and [22]Pathology, St. Vincent's Hospital; [23]Department of Haematology and Medical Oncology, Peter MacCallum Cancer Centre, Melbourne, Victoria, Australia; [24]Department of Pathology, [25]CHU Grenoble Institut National de la Santé et de la Recherche Medicale (INSERM) U823, Institute Albert Bonniot, Grenoble-Alpes University, Grenoble, France; [26]Laboratory of Oncology IRCCS Casa Sollievo della Sofferenza, San Giovanni Rotondo; [27]Laboratory for Molecular Medicine and Biotechnology, University Campus Bio-Medico, Rome, Italy; [28]Center for the Biology of Disease, VIB, Leuven; and [29]Oncology Discovery, Janssen Research and Development, A Division of Janssen Pharmaceutica NV, Beerse, Belgium

Note: Supplementary data for this article are available at Cancer Discovery Online (http://cancerdiscovery.aacrjournals.org/).

L. Fernandez-Cuesta and D. Plenker contributed equally to this work.

Corresponding Author: Roman K. Thomas, Department of Translational Genomics, Medical Faculty, University of Cologne, Weyertal 115b, 50931 Cologne, Germany. Phone: 49-221-478-98771; Fax: 49-221-478-97902; E-mail: roman.thomas@uni-Koeln.de

doi: 10.1158/2159-8290.CD-13-0633

Published OnlineFirst January 27, 2014; DOI: 10.1158/2159-8290.CD-13-0633

INTRODUCTION

Lung adenocarcinomas of patients who have never smoked frequently bear kinase gene alterations, such as *EGFR* mutations and translocations affecting *ALK*, *ROS1*, and *RET* (1–6). These alterations cause "oncogene dependency" on the activated kinase and, thus, sensitivity of the tumor cells to kinase inhibitors. Patients whose tumors bear kinase gene alterations can be effectively treated with an ever-growing number of kinase inhibitors; for example, patients with *EGFR*-mutant lung cancer treated with EGF receptor (EGFR) inhibitors have a significantly longer progression-free survival compared with patients treated with conventional chemotherapy (7). Similarly, ALK and ROS1 inhibition induces clinically relevant remissions in patients bearing the respective genomic fusion (8–10). Unfortunately, despite substantive cancer genome sequencing efforts, a majority of lung tumors still lack therapeutically tractable kinase alterations (1). We therefore sought to identify novel therapeutically relevant driver alterations in otherwise driver-negative lung adenocarcinomas.

RESULTS

We collected a cohort of 25 lung adenocarcinoma specimens of never smokers that lacked mutations in *KRAS* or *EGFR*, on which we performed chromosomal gene copy-number analysis as well as transcriptome sequencing with the aim of identifying new oncogenic driver alterations. We applied a novel computational data analysis strategy that combines split-read and read-pair analyses with *de novo* assembly of candidate regions containing potential breakpoints to achieve sensitive and accurate detection of fusion transcripts (see Methods; Fernandez-Cuesta and colleagues, published elsewhere). Of the 25 samples analyzed (Supplementary Table S1), 10 carried a known oncogene. One sample exhibited *EGFR* amplification, paralleled by overexpression of the gene (Fig. 1A and Supplementary Fig. S1). We also found 3 cases each of *ALK*, *ROS1*, and *RET* fusions (Fig. 1A and Supplementary Table S2). In addition, we detected one sample carrying a novel chimeric transcript fusing the first six exons of *CD74* to the exons encoding the EGF-like domain of the neuregulin-1 (NRG1) III-β3 isoform (Fig. 1A and B and Supplementary Table S2). This fusion raised our interest because *CD74* is part of recurrent fusions affecting the *ROS1* (3) kinase in lung adenocarcinoma, and because *NRG1* encodes a ligand of ERBB receptor tyrosine kinases, which are also frequently affected by genome alterations in this tumor type. NRG1 provides the ligand for ERBB3 and ERBB4 receptors (11). The NRG1 isoform present in our fusion transcript belongs to the type III and carries the EGF-like domain type β, which has higher affinity to the receptors than the α-type (12). NRG1 type III expression is mostly limited to neurons and is the only isoform displaying this degree of tissue-specific expression (13). Only the sample carrying the *CD74–NRG1* fusion exhibited high expression of the NRG1 III-β3 isoform [74 fragments per kilobase per million reads (FPKM); Fig. 1C, top; Supplementary Table S3], and in this specimen there was no expression of the wild-type allele (Fig. 1C, bottom). In addition, NRG1 was generally not expressed in lung adenocarcinoma as shown by transcriptome sequencing data of our cohort of 25 lung adenocarcinomas of never smokers (Fig. 1C, top, and Supplementary Table S3), and of a cohort of 15 unselected lung adenocarcinomas (Fig. 1C, top, and Supplementary Table S4). The fusion resulted from a somatic genomic event as *CD74–NRG1* fusion FISH and *NRG1* break-apart FISH revealed rearrangements in the respective chromosomal regions in the tumor cells, but not in surrounding nontumoral cells (Fig. 1D and Supplementary Fig. S2). Furthermore, by applying hybrid-capture–based massively parallel genomic sequencing (Fig. 1D and Supplementary Table S5), we found five and two reads spanning and encompassing the chromosomal breakpoint (chr5:149,783,493 and chr8:32,548,502), respectively.

We next performed reverse transcriptase PCR (RT-PCR) using primers specific for the chimeric transcript to identify additional tumors bearing the fusion in a set of 102 pan-negative adenocarcinomas of never smokers (wild-type for *EGFR*, *KRAS*, *BRAF*, *ERBB2*, *ALK*, *ROS*, and *RET* genes). We identified four additional tumors carrying the fusion (Supplementary Table S6), which were also confirmed by break-apart FISH. All 5 cases (including the index case) occurred in invasive mucinous adenocarcinomas (IMA) of women who had never smoked (Fig. 2A). Invasive mucinous lung adenocarcinoma is highly associated with *KRAS* mutations (14). Indeed, out of 15 invasive mucinous lung adenocarcinoma specimens (all derived from an East Asian population), six carried a *KRAS* mutation (40%), and four carried the *CD74–NRG1* fusion (27%; Fig. 2B; Supplementary Table S7). We additionally tested other lung tumor subtypes (63 cases), as well as four other cancer types (21 cases) and all were negative for the fusion gene (Supplementary Table S6), suggesting a strong link between the presence of *CD74–NRG1* and invasive mucinous adenocarcinoma.

Characteristic features of type III NRG1 are cytosolic N-termini and membrane-tethered EGF-like domains (13, 15). In the case of CD74–NRG1, the part of CD74 is predicted to replace the transmembrane domain present in wild-type NRG1 III-β3, preserving the membrane-tethered EGF-like domain (Fig. 2C). To validate this prediction, we transduced NIH-3T3 cells with CD74–NRG1-encoding retroviruses, and performed flow cytometry analyses to determine the subcellular distribution of expression of the fusion protein. As expected, we observed a positive intracellular (but not extracellular) signal for CD74 (Fig. 2D, left) and a positive extracellular signal for NRG1 (Fig. 2D, right). Similar results were observed in H2052 cells (Supplementary Fig. S3). Furthermore, we were unable to detect the fusion in the supernatant of transduced cells with a polyclonal antibody raised against the EGF-like domain (data not shown). Thus, the fusion does not lead to secretion of the EGF-like domain, but probably generates a membrane-bound protein with the EGF-like domain presented on the outside of the cell.

We next analyzed the expression of ERBB receptors in the index case: *ERBB1* (*EGFR*) was almost not expressed (FPKM = 1.9; Fig. 3A; Supplementary Table S8; Supplementary Fig. S4) and not phosphorylated (Supplementary Fig. S4). In contrast, *ERBB2* was expressed (FPKM = 22.9; Fig. 3A; Supplementary Table S8) and phosphorylated (Fig. 3B, left); similar to *ERBB2*, *ERBB3* was also expressed at relatively high levels

Published OnlineFirst January 27, 2014; DOI: 10.1158/2159-8290.CD-13-0633

A

Sample	Age	Sex	Stage	Driver
Case-01	63	Female	Ia	*EGFR*-amp
Case-08	68	Male	Ia	*EML4–ALK*
Case-10	46	Female	Ia	*EML4–ALK*
Case-17	39	Female	IIIa	*EML4–ALK*
Case-06	56	Female	IIIb	*CD74–ROS1*
Case-09	60	Female	Ia	*CD74–ROS1*
Case-02	68	Female	IIIb	*EZR–ROS1*
Case-15	65	Female	IIa	*KIF5B–RET*
Case-25	75	Male	Ia	*KIF5B–RET*
Case-23	66	Female	IIIb	*CCDC6–RET*
Case-19*	64	Female	Ib	*CD74–NRG1*
Case-03	72	Female	IV	
Case-04	74	Male	IV	
Case-05	50	Female	IV	
Case-07	70	Female	Ia	
Case-11	79	Female	IIa	
Case-12	72	Male	IV	
Case-13	59	Male	Ib	Unknown
Case-14	63	Female	IIIa	
Case-16	48	Male	IIIb	
Case-18	71	Female	IIIa	
Case-20	74	Female	IIIa	
Case-21	73	Male	Ib	
Case-22	80	Female	Ib	
Case-24	66	Female	IIIa	

*, Index case (Caucasian, invasive mucinous adenocarcinoma)

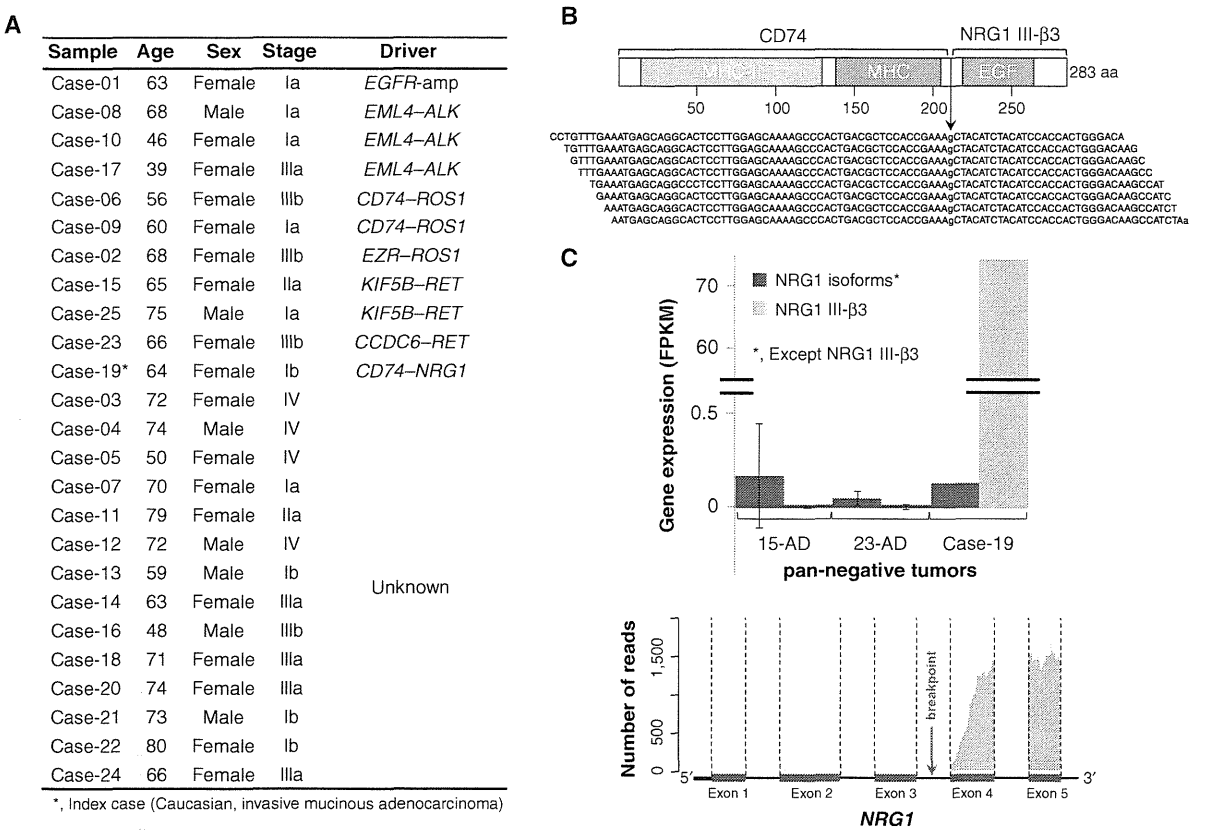

Figure 1. Identification of the *CD74-NRG1* fusion gene. **A,** overview of driver genes detected in a cohort of 25 *EGFR*- and *KRAS*-negative lung adenocarcinomas of never smokers. **B,** detection of *CD74-NRG1* fusion transcript by transcriptome sequencing. Schematic representation of the fusion transcript domains and some of the transcriptome sequencing reads spanning the fusion point. **C,** expression levels of *NRG1* isoforms in 15 unselected and 23 pan-negative lung adenocarcinomas (AD; wild-type for *EGFR, KRAS, BRAF, ERBB2, ALK, ROS,* and *RET*), and, in the index case, inferred from transcriptome sequencing data. Average FPKM values are shown (top). RNAseq analysis for *NRG1* reads to show where the breakpoint of *CD74-NRG1* occurs. The dip in exon 4 represents reads of the fusion that could not be mapped. No reads could be mapped to exons 1–3 (bottom). **D,** top, the genomic intron/exon structure of the *CD74* (in green) and the *NRG1* locus (in orange) with the genomic breakpoints marked in red. Sequencing reads were obtained from hybrid-capture–based genomic sequencing of 333 genes using genomic DNA of the index case (see Methods). The breakpoint-spanning reads are shown by means of the Integrative Genomics Viewer (www.broadinstitute.org/igv/) focused on the *CD74* gene (bottom). The gray area of the read is aligned to the *CD74* reference sequence. Colored area on the right indicates bases not matching the *CD74* reference sequence. Sequence comparison reveals alignment to the *NRG1* reference sequence. Encompassing reads whose mate pairs are mapped to the *NRG1* locus on chromosome 8 are displayed in dark purple. Bottom, a representative picture of *NRG1* break-apart FISH. Arrows, break-apart signals.

Published OnlineFirst January 27, 2014; DOI: 10.1158/2159-8290.CD-13-0633

A

Sample	Age	Sex	Stage	Smoking status	AD subtype
Index-case	64	Female	Ib	Never	Invasive mucinous
Case-A	73	Female	Ia	Never	Invasive mucinous
Case-B	72	Female	Ia	Never	Invasive mucinous
Case-C	66	Female	Ia	Never	Invasive mucinous
Case-D	31	Female	Ia	Never	Invasive mucinous

EGFR, KRAS, BRAF, HER2, ALK, ROS, RET negative

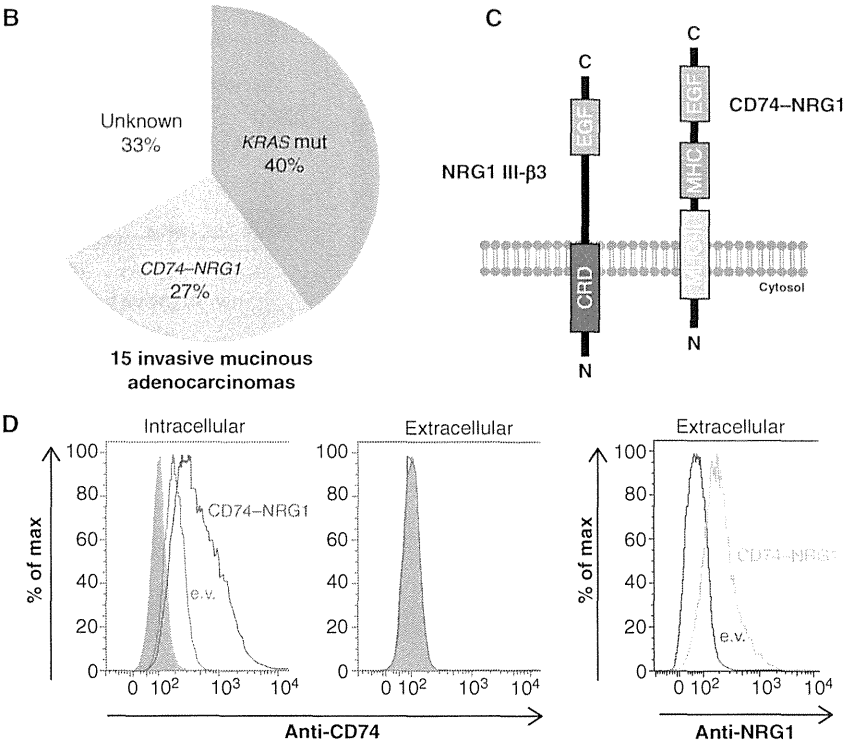

Figure 2. Association of *CD74-NRG1* with invasive mucinous adenocarcinoma, and membrane localization of the fusion protein. **A,** clinical characteristics of the index case and the 4 additional cases found to harbor *CD74-NRG1*. **B,** frequency of *KRAS* mutations and *CD74-NRG1* rearrangements in a cohort of 15 IMA tumors (East Asian population). **C,** schematic representation of wild-type NRG1 III-β3 and predicted CD74-NRG1 fusion protein in the cellular membrane. **D,** intracellular and extracellular staining of CD74 (left), and extracellular staining of NRG1 (right) in CD74-NRG1-transduced NIH-3T3 cells, detected by flow cytometry. The percentage of max is the number of cells in each bin divided by the number of cells in the bin that contains the largest number of cells. e.v., empty vector control.

(FPKM = 22.8; Fig. 3A; Supplementary Table S8) and also phosphorylated (Fig. 3B, right). *ERBB4* was not expressed in the index case (FPKM = 0.2; Fig. 3A; Supplementary Table S8). To our surprise, expression of phosphorylated ERBB3 (p-ERBB3) was almost exclusively restricted to fusion-positive cases, as determined by an immunohistochemical analysis of a tissue microarray containing 241 unselected adenocarcinomas. Although a positive signal was detected for p-ERBB3 in the five CD74-NRG1-positive invasive mucinous adenocarcinomas, only six of 241 unselected adenocarcinomas exhibited detectable levels of p-ERBB3 ($P < 0.0001$; Fig. 3C). Together, these observations support the notion that CD74-NRG1 might provide the ligand for ERBB2–ERBB3 heterodimers, thus activating the phosphoinositide 3-kinase (PI3K)-AKT pathway, as previously shown for wild-type NRG1 (16).

To formally test this hypothesis, we transduced different cell lines with retroviruses encoding CD74–NRG1 and performed Western blot analyses under starving conditions. Because NIH-3T3 cells have low-to-absent expression of ERBB receptors, and NIH-3T3 cells ectopically expressing ERBB2 and ERBB3 are already oncogenic (Supplementary Fig. S5), we decided to use H322 and H1568 lung cancer cell lines expressing normal ERBB2 and ERBB3 levels instead. We transduced these cell lines with either an empty vector, a virus containing the full fusion transcript, or a virus containing a truncated version of the fusion lacking the EGF-like domain (Supplementary Fig. S6). We observed that H322 and H1568 cell lines ectopically expressing CD74–NRG1 showed increased levels of p-ERBB2, p-ERBB3, p-AKT, and p-S6K when compared with the empty vector control (Fig. 3D). Furthermore, both p-ERBB3 and

Published OnlineFirst January 27, 2014; DOI: 10.1158/2159-8290.CD-13-0633

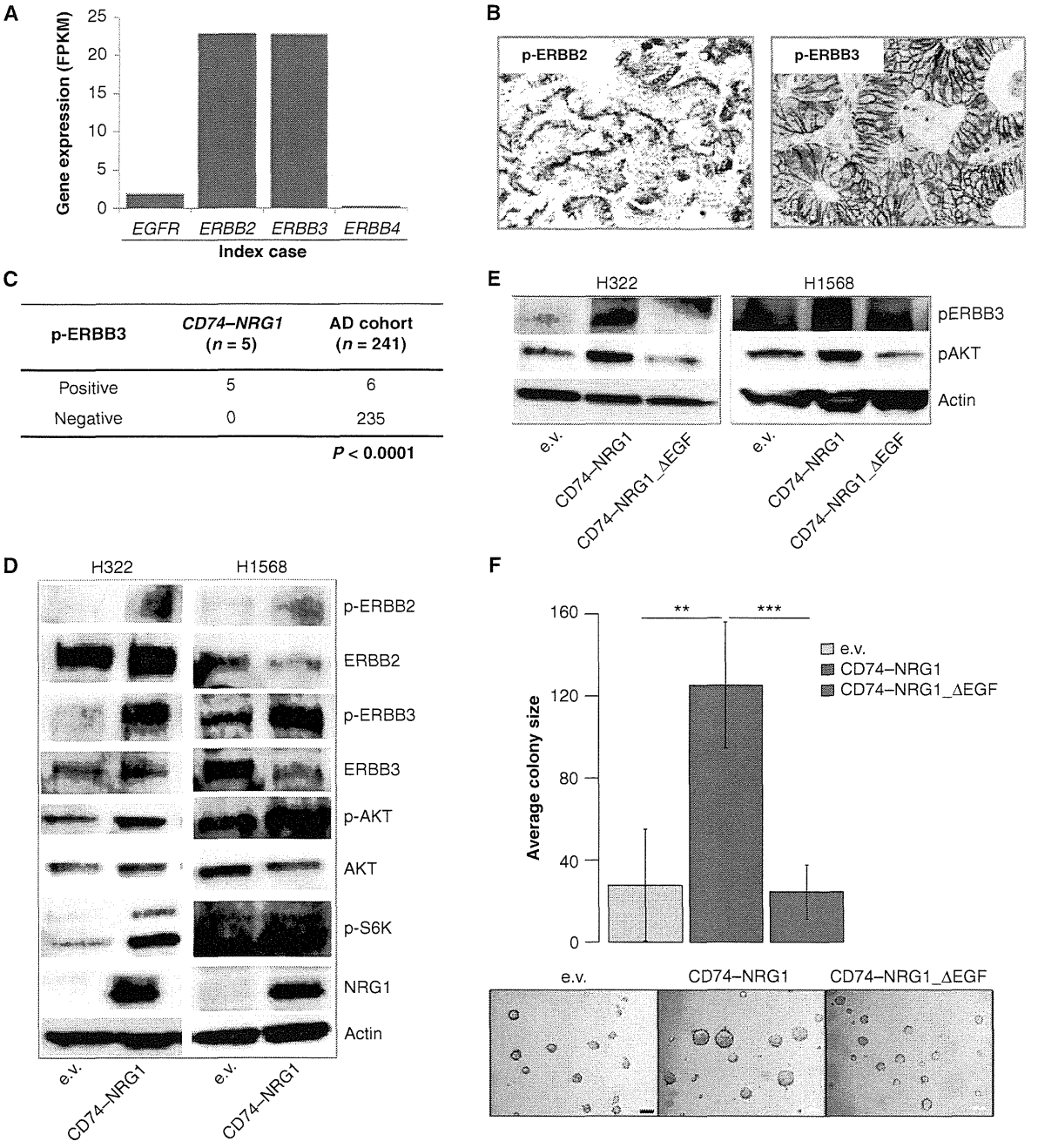

Figure 3. Functional relevance of CD74-NRG1. **A,** expression levels of ERBB receptors in the index case inferred from transcriptome sequencing data. FPKM values are shown. **B,** levels of p-ERBB2 and p-ERBB3 detected by immunohistochemical analysis in a CD74-NRG1-positive case using and antibody directed against ERBB2 Tyr1221/1222 and ERBB2 Tyr1289. **C,** the same p-ERBB3 antibody was used to stain a tissue microarray composed of 241 lung adenocarcinomas. The frequency of p-ERBB3-positive cases in this cohort versus the five CD74-NRG1-positive samples is shown ($P < 0.0001$). **D,** activation of the PI3K-AKT pathway detected by Western blot analysis of H322 and H1568 lung cancer cells transduced with retroviruses encoding CD74-NRG1 or the empty vector control (e.v.). **E,** levels of p-ERBB3 and p-AKT measured by Western blot analysis in the presence of an empty vector, CD74-NRG1, or a truncated version lacking the EGF-like domain (CD74-NRG1_ΔEGF). **F,** anchorage-independent growth of H1568 cells expressing an empty vector, CD74-NRG1, or a truncated version lacking the EGF-like domain (CD74-NRG1_ΔEGF). Top, the average colony size for the three conditions, with error bars representing standard deviations. The experiment was performed with two independent transductions for a total of four times. **, $P < 0.01$; ***, $P < 0.001$. Bottom, representative pictures of the colony formation assay. Please note that H1568 cells are oncogenic and form small colonies without any manipulation.